CO4-1 Evaluation of Gamma-ray Induced Current on Triaxial Cables

Y. Gotoh, N. Sato[1], Y. Okuno[2], M. Imaizumi[3], M. Akiyoshi[4], T. Kobayashi[5] and T. Okamoto[6]

Graduate School of Engineering, Kyoto University
[1]Institute for Integrated Radiation and Nuclear Science, Kyoto University
[2]Institute for Materials Research, Tohoku University
[3]Research and Development Directorate, Japan Aerospace Exploration Agency
[4]Radiation Research Center, Osaka Prefecture University
[5]Center for Advanced Photonics, RIKEN
[6]National Institute of Technology, Kisarazu College

INTRODUCTION: In nuclear decommissioning of Fukushima Daiichi Nuclear Power Plant, monitoring of the dose rate of irradiation is necessary. The present study proposes use of solar cell as dosimeter [1]. To monitor the output of the solar cell, it should be confirmed that the signal is not modified by some external circumstances such as electric noise or radiation induced current. In the previous report [2], the current induced on a coaxial cable was investigated, but exact evaluation of the gamma-ray induced current as a function of the dose of irradiation was not possible. The reasons were: lack of the information on dose rate distribution of the space where the cable occupies, and difficulties in fixing the cable to a pre-determined position due to large length of the cable. In this study, these problems were overcome in a following manner. The cable was wound on a wooden frame to identify the position of the cable. The dose rate was measured with the solar cell dosimeter that is currently under development. With these improvements, the current induced on the triaxial cable was investigated.

EXPERIMENTS: Gamma-ray irradiation was performed at the Co-60 gamma-ray irradiation facility, Institute for Integrated Radiation and Nuclear Science. A solar cell dosimeter was prepared in a small can made of stainless steel in which an InGaP solar cell with an area of 1 cm^2 [3] was placed. Prior to the measurements, the sensitivity of the dosimeter was calibrated at the position where the dose of irradiation has been measured. The cable used in the present study was a 1.5D type triaxial cable. A 15 m-long triaxial cable was wound on the wooden frame with the height of 20 cm and the width of 40 cm. The cable was placed at 60 cm away from the gamma-ray source to achieve uniform dose rate for the entire cable. The obtained values of the dose rate of irradiation was 60 Gy h^{-1} at the front face of the wound cable and 40 Gy h^{-1} at the back face. One end of the cable was open and the other end was connected to a pico-ammeter located at the outside of the irradiation room to measure the gamma-ray induced current. Unlike the common usage of the cable, the signal transfer was made with the core wire and the outer shield of the cable; inner shield was either floated or grounded. Since it has already been known that the cable shows a transitional current when the irradiation starts, the induced currents were observed for more than 20 hours. To check the current induced at the cable connecting the sample cable and the pico-ammeter, another triaxial cable was put aside of the sample cable.

RESULTS: Observation started with the inner shield floated. When starting irradiation, the cable showed a large positive transition current as observed so far. Figure 1 shows the variation of the induced current as a function of time of irradiation. The peak current was about 300 pA. It decayed within several minutes, but showed a negative value of -5 pA. The current gradually decreased, but after 21 hours radiation, it showed -3.5 pA, as shown by the dot in Fig. 1. Considering that the induced current once decreased to less than -3 pA, the current would increase again. Connecting the inner shield to ground, the current increased to approximately -10 pA, followed by a relatively rapid decay (time constant of decay, less htan 10 min) to -8.2 pA. Opening the inner shield, the current approached to zero, but rapidly came to -3.8 pA.

It was concluded that the cable showed the cable showed the gamma-ray irradiated charge of 0.14 – 0.21 pC Gy^{-1} cm^{-1} when the inner shield was floated, and 0.33 – 0.49 pC Gy^{-1} cm^{-1} when the inner shield was grounded. These values are lower than the reported values [4].

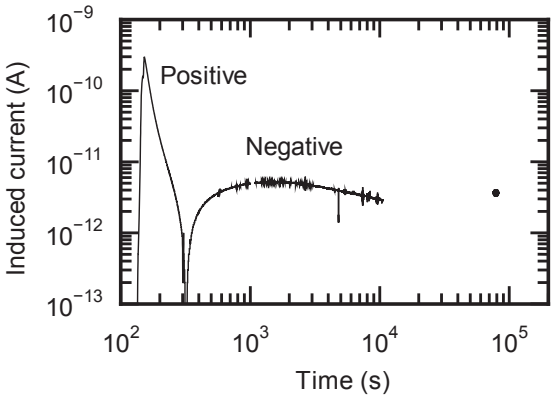

Fig. 1. Observed current under gamma-ray irradiation. The dot shown in the right-hand side is the current observed after 21 hour irradiation.

ACKNOWLEDGMENTS: This work was financially supported by the Nuclear Energy Science & Technology and Human Resource Development Project (through concentrating wisdom) from JAEA/CLADS.

REFERENCES:

[1] T. Okamoto *et al.*, Jpn. J. Appl. Phys. **60**, SBBF02 (2021).
[2] Y Gotoh *et al.*, KURNS Progress Report, CO4-20 (2020).
[3] M. Imaizumi *et al.*, Prog. Photovolt: Res. Appl. **25**, 161 (2017).
[4] K. Yahagi and A. Danno, J. Appl. Phys. **31**, 734 (1960).

CO4-2

Damage Evolution in Neutron-irradiated Metals during Neutron Irradiation at Elevated Temperatures

I. Mukouda and Q. Xu[1]

Hiroshima International University
[1]Institute for Integrated Radiation and Nuclear Science, Kyoto University

INTRODUCTION: It is accumulated an attention that a damage structure in neutron irradiated metals differs if the temperature is varied during irradiation [1]. Especially effect of lower temperature irradiation on the development of damage structure in metals which are irradiated subsequently at higher temperature was reported to be remarkable because the point defects nucleate at lower temperature more frequently during an irradiation. Recently the temperature controlled irradiation devices were developed at KUR [2]. It becomes possible to irradiate continuously at two stage of temperature. In the present work, effects on damage formation in neutron-irradiated copper for the temperature variation were examined for an irradiation at low fluence regime.

EXPERIMENTS: Copper disks of 3mm in diameter were prepared with 99.999% nominal purity specimen. Before an irradiation, they were annealed for 5 hours at 1273 K in vacuum of 10^{-5} Pa. Specimens were irradiated by fission neutrons in a temperature controlled irradiation device in KUR-SSS. In the previous temperature varying irradiation, specimens were irradiated at first at 473K and 573K. After a radiation cooling, they were observed by electron microscopy. A TEM observation was carried out using g = (002) reflection with (g, 5g) condition for the specimens of (110) configuration. Voids were observed in a bright field image by taking a slightly under forcussed image. A triangular image was taken as stacking fault tetrahedra (SFT) and diffused dot image was tentatively taken to be an interstitial cluster.
Present temperature varying irradiation, specimens were irradiated at 473K-6hrs/573K-40hrs, 473K-23hrs/ 573K-23 hrs and 473K-6 hrs/573K-20 hrs at 1MW. TEM observation are carried out recently.

RESULTS: In 473K-10hrs/573K-10hrs irradiation at 5MW, the number density of voids and SFT was smaller than those of constant temperature irradiation at 573K. Especially the decrease of number density of voids was significant [3]. shows dislocations in the specimen. Dislocations were not decorated by interstitial clusters. The number density of SFT was smaller than the value in copper which were irradiated at constant temperature of 573 K. Only one void was observed in specimens as in this picture, which means the formation of voids was suppressed significantly by the present temperature elevation irradiation.
Neutron-irradiated copper at 573K for 10 hours at 5MW, the dislocation structure show no decorated interstitial clusters around dislocation. Interstitial clusters, which were accumulated along dislocation lines, were unified to grow to dislocations. This makes development of complicated structure of dislocations as reported by Mukouda and Shimomura [4].
The suppression of void formation in temperature-varied irradiation suggests that the nucleation of voids during a constant temperature irradiation at 573K in copper occurs during the period of dislocation decoration by interstitial clusters.
In 473K-6hrs/573K-40hrs irradiation at 1MW, the number density of voids and SFT was significant smaller than those of constant temperature irradiation at 573K, some voids were observed. In 473K-6hrs/573K-40hrs irradiation at 1MW as shown in Fig. 1(a). In 473K-23hrs/ 573K-23hrs irradiation at 1MW as shown in Fig. 1(b). Total dose were same as Fig. 1(a) and (b). The suppression of void and small clusters formation in temperature-varied irradiation.

REFERENCES:

[1] N. Yoshida, Q. Xu, H. Watanabe, Y. Miyamoto and T. Muroga, J. Nucl. Mater., 212-215 (1994) 471.
[2] T. Yoshiie, Annual Reports of KUR (1998).
[3] I. Mukouda and Q. Xu, KURNS progress report 2018, Co4-7.
[4] I. Mukouda and Y. Shimomura, Material Science & Engineering A309-310 (2001) 190-197.

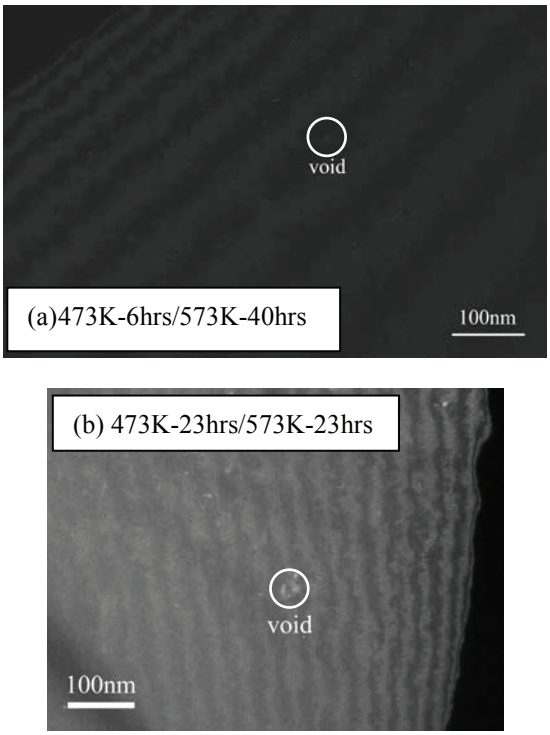

Fig. 1.Damaage structures were observed. The irradiation was carried out at first at 473K and subsequently at 573K at 1MW. Only one void was observed in white circle.

CO4-3 Lattice strain of Al by ECAP process

K. Iwase, K. Mori[1]

Department of Materials Science and Engineering, Ibaraki University

[1]Institute for Integrated Radiation and Nuclear Science, Kyoto University

INTRODUCTION: Equal channel angular pressing (ECAP) has been proved to be an efficient approach to obtain ultrafine-grained materials, and can produce huge plastic strain without changing the section shape of ob-jective materials. Large quantity of investigations about ECAP (Fig. 1) process applied to various materials have been carried out [1–3]. Severe plastic deformation (SPD) has been used to produce ultrafine-grained materials.[4] Equal-channel angular pressing (ECAP) is a processing technique used to achieve SPD. It has been reported that the lattice strain and dislocation density initially increases to a saturation level and then decreases with repetition of ECAP cycles.

In this study, we investigated the lattice strain of Al after ECAP process by neutron diffraction.

EXPERIMENTS: NPD data were collected by using the step-scan mode of a diffractometer (B-3) [5] with 1.0294
Å wavelength. Data analysis was carried out by Rietveld refinement program RIETN-FP [6]. The size of ingot Al is 10×10×5 mm.

RESULTS: Fig. 2 shows the Rietveld refinement pattern of Al before ECAP process. The calculated data fitted well to the observed data. The refined lattice parameter was a = 4.06504(12) Å. Fig. 3 shows the Al block sample after ECAP process, which indicates similar pattern in comparison with before ECAP process. The intensity of Bragg peaks of ECAP sample was smaller than that of Al before ECAP. The refined lattice pa-rameter a was 4.06391(15) Å, which was almost same as before ECAP sample. We determined the full width half of maximum (FWHM) of 111 reflection. The FWHM value is affected on the lattice strain and dis-location density. The FWHM of Al and Al after ECAP was 0.8° and 1.0°, which suggests that dislocation density increases by ECAP process.

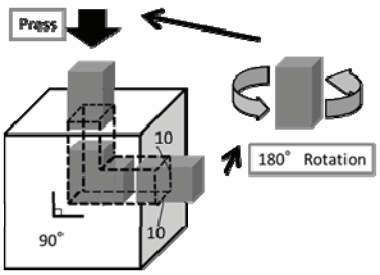

Fig. 1 ECAP process.

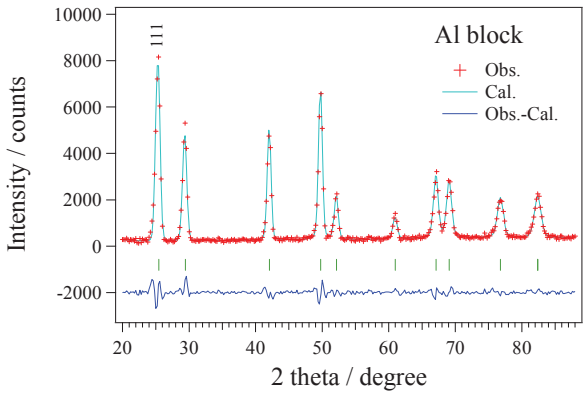

Fig. 2 Rietveld refinement pattern of Al.

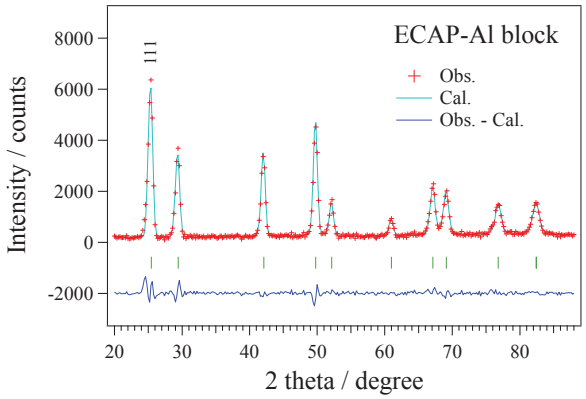

Fig. 3 Rietveld refinement pattern of Al after ECAP process.

REFERENCES:

[1] Z. Zhang *et al.*, Corrosion Science, **49** (2007) 2962-2972.
[2] V.M. Segal, Mater. Sci. Eng. A **271** (1999) 322–333.
[3] J. Wang *et al.*, J. Mater. Res. **8** (1993) 2810–2818.
[4] T. Ishibashi et al., Mater. Trans. 54 (2013) 1562-1569.
[5] K. Mori et al. *Conf. Proc.* 33 (2021) 011093.
[6] F. Izumi and K. Momma, Solid State Phenom., **130**, 15–20 (2007).

CO4-4 Synthesis of complex nanoparticles in water by γ-ray irradiation reduction

F.Hori, K.Zhu, T.Yamada[1], T.Matsui[1], N.Taguchi[2], S.Tanaka[2] and Q.Xu[3]

Dept. of Engineering, Osaka Prefecture University

[1]*Center for Advanced Education of Entrepreneurship and Innovation, Osaka Prefecture University*

[2]*AIST, Kansai Center*

[3]*Institute for Integrated Radiation and Nuclear Science, Kyoto University*

INTRODUCTION: It is known that metal nanoparticles (NPs) have some specific properties, which are not appeared in bulk materials such as catalytic activities, magnetic properties, electric conductivity and light absorption. These properties depend on its size, shape, structure, chemical composition and so on. They have many possibilities to applied for various industrial fields. However, it is not easy to fabricate multi elemental alloy NPs controlling with their structure. Almost fabrication method of NPs with commercially is based on equilibrium chemical reaction in ionic solution with reduction additive. Recently, some reports show that it is possible to fabricate metal NPs under irradiation reduction fields such as ultrasonic, solution plasma, electron beam, ion beam and gamma-ray [1]. By using this radiation reduction method, we have been trying to synthesize various kinds of metal nanoparticles with size and shape. So far, we have successfully synthesized pure Cu and Cu-Au alloy nanoparticles in water by gamma-ray reduction method. In this study, we have studied the reduction rate dependence for the synthesis of various alloy nanoparticles by the reduction under electron and gannma-ray irradiation.

EXPERIMENTS:

Aqueous solutions with various ternary combination of a given concentration of copper complex ($(CH_3COO)_2Cu \cdot H_2O$), $AgNO_3$, NiCl, $Na[AuCl_4]$ and $PdCl_2NaCl_3H_2O$ with an additive of polyvinyl (PVP) and 8.5 vol% ethylene glycol were prepared. The ratio of all ion concentration was adjusted to the same in the solution. The solution was argon gas purged and sealed into polystyrene vessels. They were irradiated at about 300 K with 1.17 and 1.33 MeV gamma-rays from ^{60}Co radio active source at gamma irradiation facility in KURRI, Kyoto University. The total dose was fixed to 10 kGy with the dose rate of 1.0 kGy/h. Also, same solutions were irradiated 8 MeV electron with total dose of 10kGy in about 60 sec by linear accelerator at same facility. After irradiation, the samples were measured for UV–vis absorption spectra. The structures for all colloidal products were measured by X-ray Photoelectron Spectroscopy (XPS) measurement at KEK-PF BL-27 and X-ray diffraction.

RESULTS:

Fig. 1 shows the photograph of before and after electron and gamma-ray irradiated samples. As is seen in this figure, the color of all samples was changed after irradiation, but different it between electron and gamma-ray irradiation. This result reveals that the size and/or state of synthesized particles depend on the reduction rate clearly. Fig. 2 shows the light absorption spectra of AgCuNi and AgAuCu ternary solutions after electron irradiation reduction. No clear characteristic peak of surface plasmon absorption corresponding to pure Au, Cu and Ag nanoparticles was obserbed but broad peaks appears in both samples. The origin of these peaks can not be determined, but the possibility is deduced as mixtured the elemental atoms in formed nanoparticles. XPS results show the formation of some metal bonds, such as Ag-Ni and Ag-Cu. More detailed state of nanoparticles are now examining other methods.

REFERENCE:

[1]. N.Taguchi *et al.*, Rad. Phys. Chem. 78, (2009) 1049-1053.

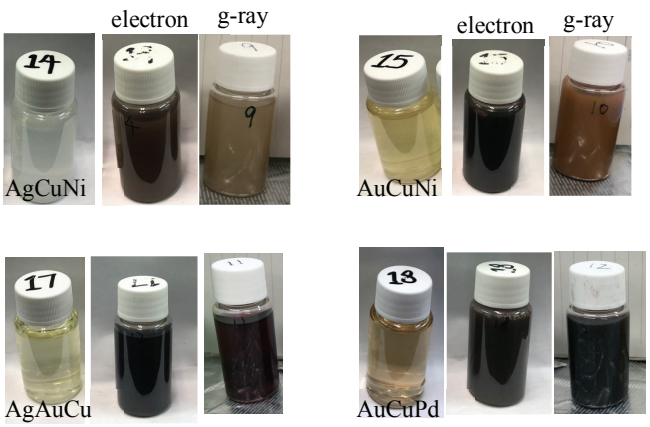

Fig.1 Photographs of electron and gamma-ray irradiation reduction samples.

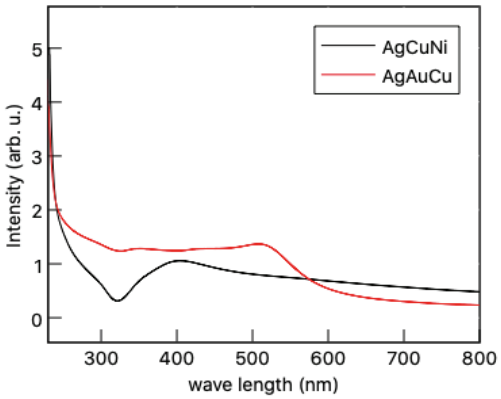

Fig. 2 UV-vis absorption spectra of electron irradiation reduction solutions including Ag, Cu, Ni and Au complexes.

CO4-5 Defect structure and characterization of electron irradiated intermetallic alloys

F.Hori, H.Ohbayashi, H.Ohtomo, Y.Morikuni, K.Ohsawa[1], Q.Xu[2] and N.Abe[2]

Dept. of Quantum & Radiation Eng., Osaka Pref. Univ.
[1]*Res. Inst. of Appl. Mech., Kyushu University*
[2]*Institute for Integrated Radiation and Nuclear Science, Kyoto University*

INTRODUCTION: In general, it is well known that intermetallic compounds have good properties such as specific strength to weight ratio, oxidation resistance and strength in elevated temperature. In addition, some of them can be applied for hydrogen storage material by production of hydride such as Mg and Ni based compound alloys. On the other hand, it found that hydrogen absorption properties in some compound alloys. It is reported that novel Ni- based alloy including defect type free volume can be used as hydrogen permeation membranes to separate H_2 from CO_2 and other gases obtained from water. We also found multi hydrogen atoms trapping at vacancy in B2 ordered FeAl alloy. It is important to clear the interaction between hydrogen and metallic materials for example hydrogen embrittlement, hydride formation and hydrogen induced transformation in hydrogen storage material. However, the nature of defects in various intermetallics is not cleared essentially. We have been studied vacancy type defects in various type of intermetallics. In this study, electron irradiation for Ni-Zr intermetallic alloy have performed in order to examine the defects and their properties.

EXPERIMENTS: $Ni_{30}Zr_{70}$ and $Ni_{63.7}Zr_{36.3}$ alloys were prepared by arc melting method in argon gas atmosphere. Sliced samples with the thickness of 0.5 mm were annealed at 1073 K for 3 h. These specimens were irradiated with 8 MeV electron up to the fluence of 4×10^{18} /cm^2 at KURRI, Kyoto University. Irradiation was carried out at about 330 K with temperature controlling water cool system. Before and after irradiation samples were measured by X-ray diffraction (XRD). Also, micro-Vickers hardness test was performed for before and after irradiation.

RESULTS: Figure 1 shows the XRD spectra of $Ni_{30}Zr_{70}$ alloy before and after electron irradiation. Before irradiation, some peaks correspond to Zr_2Ni, NiZr and pure Zr phases appeared. On the other hand, $Ni_{10}Zr_7$, Ni_7Zr_2 and $Ni_{21}Zr_8$ phases observed in $Ni_{63.7}Zr_{36.3}$ alloy. In figure 1, a peak at 36.5 corresponding to Zr phase disappeared after 4×10^{18} /cm^2 electron irradiation, but another peak at 39.5 corresponds to Zr_2Ni phase still remains after 4×10^{18} /cm^2 electron irradiation. Originally, Zr phase is not thermally equilibrium phase in this alloy. Therefore, it is considered this Zr phase disappeared by the atomic diffusion using defects introduced by irradiation. Fig.2 shows the micro-Vickers hardness change with electron irradiation fluence. It shows that this difference is originated from their phases included in. Also, it found that the trend of hardness change by the irradiation slightly different for each alloy. This is considered to be due to the difference in the nature of the hardness change of the phase including the defects introduced by irradiation.

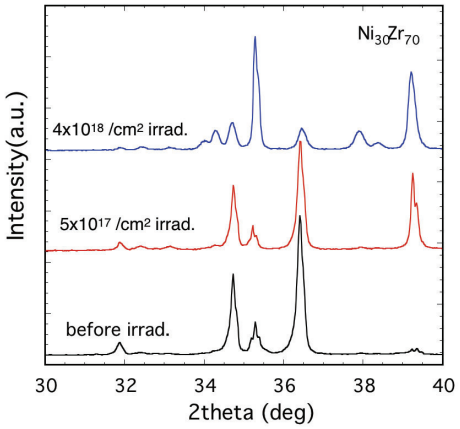

Fig. 1 XRD profiles of $Ni_{30}Zr_{60}$ alloy before and after irradiation.

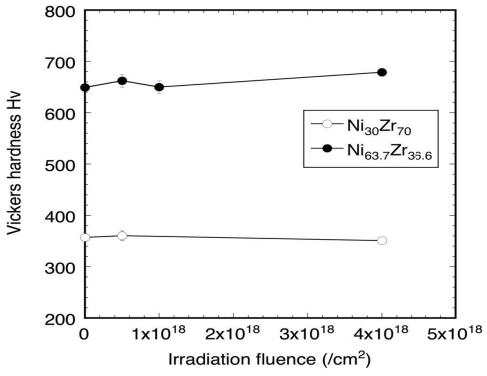

Fig. 2 Hardness chage with wlwctron irradiation fluence for NiZr alloys.

CO4-6 Study on formation mechanisms of nano-structures on Ge surfaces by low-fluence ion irradiations

J. Yanagisawa, T. Furukawa, Q. Xu[1], A. Yabuuchi[1], K. Takamiya[1], and A. Kinomura[1]

School of Engineering, The University of Shiga Prefecture
[1]*Institute for Integrated Radiation and Nuclear Science, Kyoto University*

INTRODUCTION: We have been studying the formation mechanisms of nano-structures on Ge wafer surfaces by ion irradiations using the positron annihilation methods. A peak of the S (line shape) parameter of the positron annihilation was observed by 25 or 50 keV Ar^+ irradiations at ion fluences of $1 \times$ or 5×10^{16} cm^{-2} [1] and 0.5 or 4 keV Ga^+ irradiations at a fluence of 1×10^{15} cm^{-2} [2], indicating the formation of the atomic vacancies and/or voids formed inside regions of the Ge surfaces by the Ar^+ or Ga^+ irradiations. On the other hand, no such peak of the S parameter was observed for the 0.5 keV Ga^+ irradiation at a fluence of 1×10^{14} cm^{-2} [2], indicating that the ion irradiation with such lower energy and/or lower ion fluence induces no damage on Ge surfaces. To study the influences of the lower energy ion irradiations, the effect of the plasma treatment on the surface was investigated as an example of the lower ion irradiation. Ions, as well as radicals, are the main components of plasma, therefore the sample surfaces might be influenced by ions during the plasma treatment. In the present study, we have measured the S parameters for the Si surfaces treated by oxygen plasma.

EXPERIMENTS: Chips of a Si (100) wafer with a size of about 18 mm × 18 mm were exposed to the RF (radio-frequency) plasma at a power of 5 or 100 W with the oxygen gas pressure of 5 or 20 Pa for 30 min. After the treatment, the thickness of the oxide films was measured by an ellipsometer. Table 1 shows the results for the Si samples treated with different plasma conditions, as well as un-treated Si sample as a reference. From this results, thin oxide films were formed for plasma treated samples, indicating that the Si surface was surely influenced by the oxygen ions, as well as oxygen radicals. We have measured the influences of the damages (S parameters) induced by oxygen plasma using the KUR slow positron beam system.

Table 1. O_2 plasma conditions for Si oxidation and measured thickness of SiO_2. The oxidation time was 30 min. The sample #7 is a Si wafer with a natural oxide film as a reference.

sample	RF power	O_2 pressure	SiO_2 thickness
#1	100 W	20 Pa	5.33 nm
#2	100 W	5 Pa	4.92 nm
#3	5 W	20 Pa	2.87 nm
#5	5 W	5 Pa	3.68 nm
#7	–	–	1.57 nm

RESULTS: Figure 1 shows the S parameters for the oxide films as a function of the positron energy. It is found that no peak in the S parameters was observed in these samples, although the oxidation was surely occurred, as shown in Table 1. This indicates that the oxygen plasma might influence on the damage of the oxide films during the oxidation process, but the amount of the damage was small enough for the detection limit of the S parameter. The value of the S parameters of the oxide films formed by larger RF power (100 W) was larger than those by smaller one (5 W), indicating that the acceleration energy of the ion was smaller for smaller RF power. For sample #3, it is observed that the value of S parameter was smaller than that of un-treated Si. The reason of it is not clear at present.

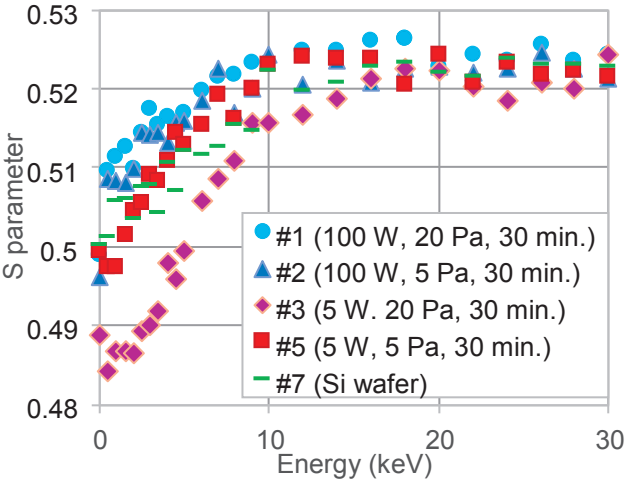

Fig. 1. S parameters for O_2 plasma treated (#1 - #5) and un-treated (#7) Si wafer samples as a function of positron energy.

CONCLUSION: To investigate the effect of damage on surfaces induced by lower energy ion irradiation at lower fluence, oxygen plasma-treated (that is, including low-energy oxygen ion irradiation) Si surface was used in the present study. From the observed S parameters, it is found that almost no damage was induced inside the oxide films by such plasma treatment.

REFERENCES:

[1] J. Yanagisawa, Q. Xu, A. Yabuuchi, K. Takamiya, and A. Kinomura, KURNS Progress Report 2018 (Kyoto University), CO4-15(30037).
[2] J. Yanagisawa, R. Tsukamoto, K. Ishihara, Q. Xu, A. Yabuuchi, K. Takamiya, and A. Kinomura, KURNS Progress Report 2019 (Kyoto University), CO4-16 (31097).

CO4-7 PAC Spectra of the ^{111m}Cd Probe in $Cd_{0.25}Fe_{2.75}O_4$

W. Sato[1,2,3], M. Fujii[2], M. Konaka[3], T. Ito[2], S. Komatsuda[4], and Y. Ohkubo[5]

[1]*Institute of Science and Engineering, Kanazawa University*
[2]*Graduate School of Science and Technology, Kanazawa University*
[3]*College of Science and Engineering, Kanazawa University*
[4]*Institute of Human and Social Sciences, Kanazawa University*
[5]*Institute for Integrated Radiation and Nuclear Science, Kyoto University*

INTRODUCTION: Spinel oxides exhibit various physical properties depending on the constituent metal elements and on their residential positions: the tetrahedral *A* site and octahedral *B* site. Among numerous spinel compounds, iron-based oxides are most promising for application to future spintronic devises; it is therefore very important to obtain microscopic information on their local fields which directly affects their bulk physical properties. In the course of our previous work to measure the local filed in a cadmium ferrite ($CdFe_2O_4$) by means of perturbed angular correlation (PAC) spectroscopy with the ^{111m}Cd probe, we obtained an unexpected spectrum without a defined oscillatory structure as shown in Fig. 1(a) [1]. In general, this kind of spectral pattern is ascribable (1) to spin relaxation of the probe nucleus induced by dynamic perturbation from extranuclear field and/or (2) to damping of the oscillation by a wide distribution of the frequency of the nuclear spin precession. In order to provide insight into the phenomenon, we have further investigated the local fields in cadmium ferrites having intermediate cadmium content between Fe_3O_4 and $CdFe_2O_4$, $Cd_xFe_{3-x}O_4$. Here, part of a preliminary result for $Cd_{0.25}Fe_{2.75}O_4$ is reported.

EXPERIMENTS: Neutron irradiation was performed for cadmium oxide (CdO) enriched with ^{110}Cd in Kyoto University Reactor to produce radioactive ^{111m}Cd by a neutron capture reaction. The radioactive Cd(^{111m}Cd)O powder was mixed well with stoichiometric amounts of CdO and Fe_3O_4 in an agate mortar. The mixture was then pressed into a disk, sealed in a quartz tube in vacuum, and sintered in air at 1373 K for 45 min.

PAC measurements were carried out for the ^{111m}Cd($\rightarrow^{111}$Cd) probe on the 151-245 keV cascade γ rays with the intermediate state of $I = 5/2$ having a half-life of 85.0 ns. In the present work, we obtained the perturbed angular correlation as a function of the time interval of the cascade γ-ray emissions by the following expression:

$$A_{22}G_{22}(t) = \frac{2[N(\pi,t) - N(\pi/2,t)]}{N(\pi,t) + 2N(\pi/2,t)}, \qquad (1)$$

where A_{22} denotes the angular correlation coefficient, $G_{22}(t)$ the time-differential perturbation factor as a function of the time interval t between the cascade γ-ray emissions, and $N(\theta, t)$ the number of the delayed coincidence events observed at an angle θ. The measurements were performed at different temperatures.

RESULTS: The PAC spectra of ^{111m}Cd($\rightarrow^{111}$Cd) in $Cd_{0.25}Fe_{2.75}O_4$ are shown in Fig. 1(b) and 1(c). The spectrum obtained at room temperature (Fig. 1(b)) exhibits oscillatory structure reflecting static interaction with supertransferred magnetic hyperfine field from Fe ions, which is analogous to those observed for Fe_3O_4 [2]. The gradual damping of the oscillation could be attributed to distribution of constituent Cd ions. What should be noted is the spectrum in Fig. 1(c) obtained at 773 K ($> T_C$ = 753 K). It was analyzed by assuming a widely distributed electric quadrupole frequency caused by the electric field gradient produced by extranuclear charge distribution. The spectrum is similar to that in Fig. 1(a), leaving a possibility that the damping arises from the distribution of Cd ions. However, a distinct difference is that hard-core like anisotropy still remains in the spectrum in Fig. 1(c), whereas that in Fig. 1(a) hardly does. The cause of the the relaxing trend is still unknown; however, higher-temperature spectra possibly provide a clue to this intriguing phenomenon.

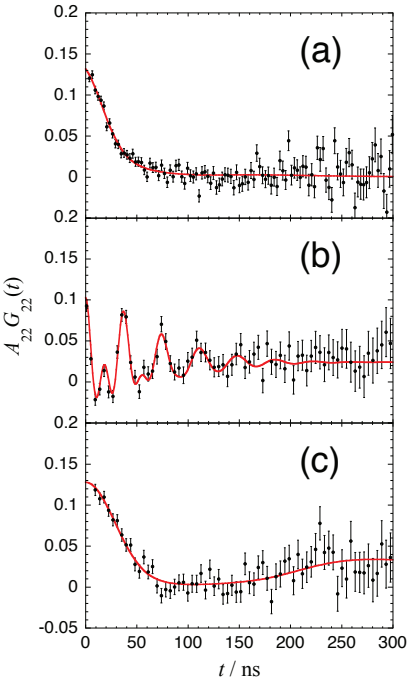

Fig. 1. PAC spectra of ^{111m}Cd($\rightarrow^{111}$Cd) (a) in R.T. $CdFe_2O_4$, (b) in R.T. $Cd_{0.25}Fe_{2.75}O_4$, and (c) in 773-K $Cd_{0.25}Fe_{2.75}O_4$.

REFERENCES:

[1] W. Sato *et al.*, J. Radioanal. Nucl. Chem. **316** (2018) 1289-1293.
[2] W. Sato *et al.*, J. Appl. Phys. **120** (2016) 145104 (1-7).

CO4-8 Characterization of the effect of Au-ion irradiation on $GdBa_2Cu_3O_{7-\delta}$ superconducting tapes using a slow positron beam

T. Ozaki, H. Sakane[1], A. Yabuuchi[2] and A. Kinomura[2]

School of Engineering, Kwansei Gakuin University
[1]SHI-ATEX Co., Ltd.
[2]Institute for Integrated Radiation and Nuclear Science, Kyoto University

INTRODUCTION: Cuprate superconductors, RE-$Ba_2Cu_3O_{7-\delta}$ (REBCO), exhibit high-temperature superconductivity and is expected to be useful for magnetic coils. Critical current properties in magnetic fields are improved by introducing lattice defects using ion-irradiation techniques. Positrons are sensitive to vacancy-type defects, and they are useful for characterizing irradiation-induced defects. In this study, $GdBa_2Cu_3O_{7-\delta}$ (GdBCO) coated conductors (CCs), which were industrially produced with a roll-to-roll process, were irradiated with Au ions at 2 or 10 MeV and probed using a slow-positron beam.

EXPERIMENTS: The GdBCO(500 nm) CCs were irradiated with 2 MeV Au^{2+} (5.0×10^{11}, 4.0×10^{12} cm^{-2}) or 10 MeV Au^{4+} (7.3×10^{11}, 5.5×10^{12} cm^{-2}) ions. The 2 MeV and 10 MeV ions stop in the GdBCO film and penetrate the GdBCO film, respectively. The unirradiated and irradiated samples were probed by the KUR slow positron beam and the Doppler broadening of annihilation radiation (DBAR) spectra were acquired with incident positron energies E_+ varying from 0.03 to 25 keV. The sharpness of the DBAR spectra is evaluated by a value called the *S*-parameter, which becomes generally lower when positrons annihilate in a perfect lattice, and higher when positrons are trapped into vacancies [1].

RESULTS: Figure 1 shows the *S*-parameters of the GdBCO samples before and after irradiation as functions of the incident positron energy. The *S*-parameters for all irradiated samples show a clear reduction, compared with that for the unirradiated sample. This reduction is opposite to the generally expected tendency of the *S*-parameter change caused by ion irradiation. Figure 2 shows the coincidence DBAR spectra for the unirradiated and the high-dose samples normalized to the calculated defect-free GdBCO spectrum. Vacancy clusters were detected in both samples. These results suggest that the size of the newly-formed defects induced by the irradiation is smaller than that of the vacancy clusters initially contained in the samples.

The relation between the *S*-parameter of the GdBCO layer obtained from the VEPFIT analysis and the value of T_c is plotted in Fig. 3. We found that irradiation-induced vacancy-type defects cause a reduction in T_c, demonstrating that a slow positron beam can be a useful tool for characterizing the effects of ion irradiation on commercial superconducting CCs that contain vacancy clusters.

REFERENCES:

[1] R. W. Siegel, Ann. Rev. Mater. Sci., 10 (1980) 393−425.
[2] A. Yabuuchi *et al.*, Appl. Phys. Express, **13** (2020) 123004.

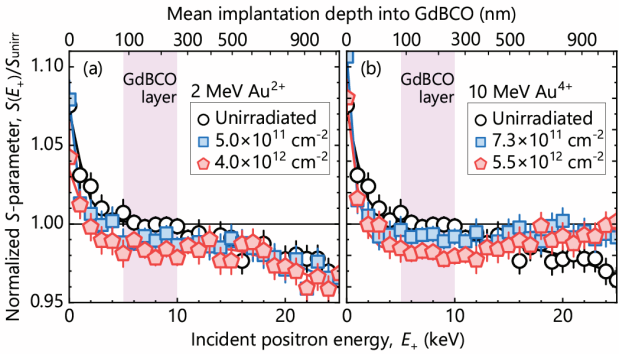

Fig. 1. *S*-parameters as functions of the incident positron energy for (a) 2 MeV Au^{2+} and (b) 10 MeV Au^{4+} irradiated GdBCO samples.[2]

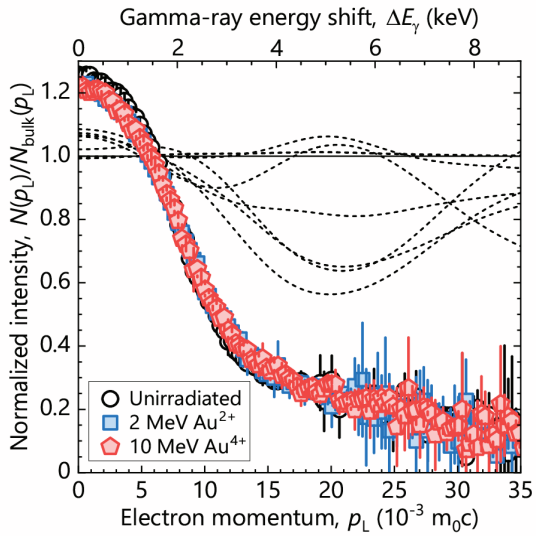

Fig. 2. Coincidence DBAR spectra obtained for unirradiated and high-dose samples. [2]

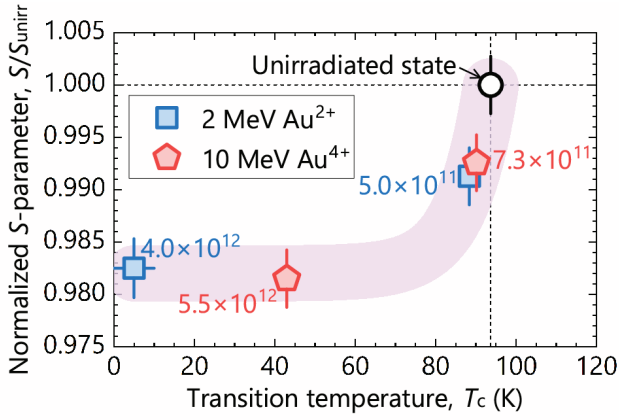

Fig. 3. Normalized *S*-parameters in the GdBCO layer as a function of the T_c. [2]

CO4-9 Local Structure of Cd Impurities doped in $Cd_xSr_{1-x}TiO_3$ Studied by TDPAC Method

S. Komatsuda, W. Sato[1] and Y. Ohkubo[2]

Institute of Human and Social Sciences, Kanazawa University
[1]*Institute of Science and Engineering, Kanazawa University*
[2]*Institute for Integrated Radiation and Nuclear Science, Kyoto University*

INTRODUCTION: Strontium titanate ($SrTiO_3$) is a cubic perovskite compound of ABO_3 type. $SrTiO_3$ doped with metal ions as impurities exhibits a wide variety of electronic properties. Especially, $SrTiO_3$ doped with trivalent metal ions at Ti^{4+} site has attracted much attention because of their excellent photocatalytic activity [1]. For a practical use of $SrTiO_3$, it is necessary to obtain more microscopic information on the impurity site. Therefore, we investigated the local structures at the In^{3+} site in $SrTiO_3$ by means of the time-differential perturbed angular correlation (TDPAC) method using the $^{111}Cd(\leftarrow{}^{111}In)$ probe. In our previous TDPAC study of $^{111}Cd(\leftarrow{}^{111}In)$ probe doped in $SrTiO_3$, three unique quadrupole frequencies were obtained. We proposed three site model of doped $^{111}In^{3+}$ sites; (i) for first components, EFG value was zero suggesting that the $^{111}Cd(\leftarrow{}^{111}In)$ probe reside at defect-free substitutional Sr^{2+} or Ti^{4+} sites in cubic $SrTiO_3$, and (ii) for second and third component, well-defined EFG values were observed, which suggests that second and third component is assignable to ^{111}In at the Sr^{2+} and Ti^{4+} site associating with defect like oxygen vacancy. Because there are a wide variety of the site occupation of $^{111}Cd(\leftarrow{}^{111}In)$ probe, information about structural and electronic properties at the impurity site is uncertain. In order to obtain further information on the local fields at Sr^{2+} or Ti^{4+} site individually, we then adopt the $^{111}Cd(\leftarrow{}^{111m}Cd)$ probe with the same valence to Sr^{2+} expecting replace only A site in $SrTiO_3$. We here report part of the result of TDPAC measurements for the $^{111}Cd(\leftarrow{}^{111m}Cd)$ in $Cd_xSr_{1-x}TiO_3$

EXPERIMENTS: Stoichiometric amount of $SrCO_3$, $CdCO_3$, and TiO_2 powders were mixed in the mortar. The powders were pressed into disks. For TDPAC measurements, about 3 mg of CdO enriched with ^{110}Cd was irradiated with thermal neutrons in a pneumatic tube at Institute for Integrated Radiation and Nuclear Science, and radioactive ^{111m}Cd was generated by $^{110}Cd(n, \gamma)^{111m}Cd$ reaction. The neutron-irradiated CdO powder was dissolved in 6M HCl and added in droplets onto the pre-sintered $Cd_xSr_{1-x}TiO_3$ disk. The disk was sintered in air at 1373 K for 90 min. The TDPAC measurement was carried out for the 151-245 keV cascade γ rays of $^{111}Cd(\leftarrow{}^{111m}Cd)$ probe with the intermediate state of $I = 5/2$ having a half-life of 85.0 ns.

RESULTS: Figure 1 shows the TDPAC spectra of (a) $^{111}Cd(\leftarrow{}^{111}In)$ in $SrTiO_3$ from our previous work, and (b) $^{111}Cd(\leftarrow{}^{111m}Cd)$ in $Cd_{0.15}Sr_{0.85}TiO_3$ at room temperature from this work. The directional anisotropy on the ordinate, $A_{22}G_{22}(t)$, was deduced with the following simple operation for delayed coincidence events of the cascade:

$$A_{22}G_{22}(t) = \frac{2[N(\pi,t) - N(\pi/2,t)]}{N(\pi,t) + 2N(\pi/2,t)}. \quad (1)$$

Here, A_{22} denotes the angular correlation coefficient, $G_{22}(t)$ the time-differential perturbation factor as a function of the time interval, t, between the relevant cascade γ-ray emissions, and $N(\theta,t)$ the number of the coincidence events observed at angle, θ. The spectra in Fig. 1 can be reproduced by a fit with three unique quadrupole frequencies. The parameters of quadrupole frequencies between the two results of Fig.1(a) and (b) were the same within the fitting error range. These observations show that local fields at the $^{111}Cd(\leftarrow{}^{111m}Cd)$ probe in $Cd_{0.15}Sr_{0.85}TiO_3$ composite oxide is identical to that at the $^{111}Cd(\leftarrow{}^{111}In)$ probe in $SrTiO_3$. It is suggested from these result that the $^{111}Cd(\leftarrow{}^{111m}Cd)$ probe also reside at three unique site; (i) for first component of zero EFGs, the $^{111}Cd(\leftarrow{}^{111m}Cd)$ probe substitutes defect-free A or B sites in cubic perovskite structure, and (ii) for second and third components of non-zero EFGs, defects were associated with the $^{111}Cd(\leftarrow{}^{111m}Cd)$ at the site of substitutional A and B site. In addition, the $Cd_{0.15}Sr_{0.85}TiO_3$ has a crystal structure of cubic perovskite of $SrTiO_3$ despite high doping concentration of Cd. For more information on the extranuclear field of the $^{111}Cd(\leftarrow{}^{111m}Cd)$ probe in $Cd_{0.15}Sr_{0.85}TiO_3$, doping rate dependence of TDPAC pattern for $Cd_xSr_{1-x}TiO_3$ is now in progress.

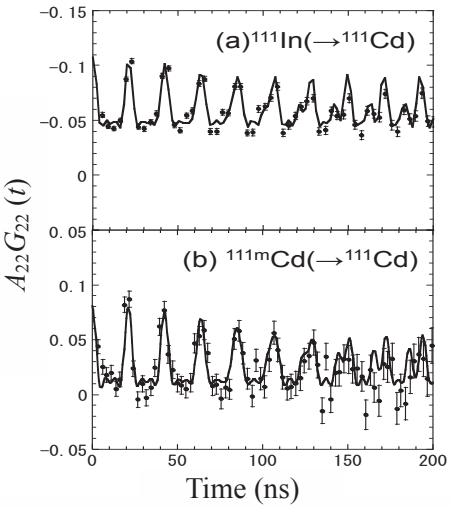

Fig. 1. TDPAC spectra of (a) $^{111}Cd(\leftarrow{}^{111}In)$ in $SrTiO_3$, and (b) $^{111}Cd(\leftarrow{}^{111m}Cd)$ in $Cd_{0.15}Sr_{0.85}TiO_3$. The measurements were perfomed at room temperature.

REFERENCES:
[1] Y. Goto *et al*., *Joule* **2** (2018) (509-520).

CO4-10 Radiophotoluminescence behavior in Cu-doped silica glass – Dose dependence and effect of heat treatment post irradiation –

Y. Takada, Y. Nishi, A. Kinomura[1], T. Saito[1], A. Okada[2], T. Wakasugi[2], K. Kadono[2]

Graduate School of Science and Technology, Kyoto Institute of Technology
[1]Institute for Integrated Radiation and Nuclear Science, Kyoto University
[2]Faculty of Materials Science and Engineering, Kyoto Institute of Technology.

INTRODUCTION: Radiophotoluminescence (RPL) or radiation-induced photoluminescence phenomena are due to emissions from luminescent centers that are generated in materials by exposure to ionizing radiation. Recently, we have found that Cu-doped aluminoborosilicate glasses exhibit remarkable RPL [1]. The mechanism for the RPL was proposed as follows. First, ionizing radiation generates electron-hole pairs in the Cu-doped glass:

$$\text{Glass} \rightarrow h^+ + e^- \qquad (1)$$

Then, the electrons are captured by Cu^{2+} ions, which are converted to Cu^+ ions:

$$Cu^{2+} + e^- \rightarrow Cu^+ \qquad (2)$$

The Cu^+ ions emit bright luminescence in the visible region by ultraviolet excitation. The reverse reaction, in which holes are captured by Cu^+ ions, can occur:

$$Cu^+ + h^+ \rightarrow Cu^{2+} \qquad (3)$$

However, in the aluminoborosilicate glasses, the copper ions mainly exist as divalent ion, Cu^{2+}, therefore, the reverse reaction hardly occurs. In addition, because of the small amount of copper incorporated in the glasses, the luminescence of Cu^+ before the irradiation is strongly suppressed. In other words, the increase in the photoluminescence is enhanced after irradiation.

In the last year, we reported that a silica glass doped with Cu exhibits RPL. The Cu-doped silica glass was prepared from a porous silica glass derived from a phase separated sodium borosilicate glass. In this research, we investigated the behaviors of the RPL in the Cu-doped silica glass in detail.

EXPERIMENTS: The Cu-doped silica glass was prepared from a porous silica glass by sintering. The method was described in the previous report in detail. The Cu-doped silica glass (abbreviated as Cu-SG, hereafter) was cut and optically polished to 1 mm thickness. The Cu-SG was exposed to γ-ray or X-ray radiations. The γ-ray irradiation experiments were performed with ^{60}Co γ-ray at the Co-60 Gamma-ray Irradiation Facility at Institute for Integrated Radiation and Nuclear Science, Kyoto University. The irradiation dose was represented as absorbed dose for water. The X-ray irradiation was performed using an X-ray source with a Rh target.

RESULTS: Figure 1 shows the photoluminescence spectra for Cu-SG measured before and after the X-ray irradiation. A luminescence band peaked at 2.5 eV was observed for the Cu-SG glass before the irradiation. However, the intensity of the band increased and the peak position shifted to 2.2 eV after the irradiation. The color of the luminescence changed from blue to yellow by the irradiation. The peak decomposition of the luminescence band after the irradiation revealed that the luminescence consists of two bands peaked at 2.5 eV and 2.1 eV and the latter newly appeared after the irradiation. Both bands are attributed to the transition of $3d^9 4s^1$ to $3d^{10}$ in Cu^+ ions. The inset in Fig. 1 shows the dose dependence of the luminescence intensity for the γ-ray irradiation. The intensity proportionally increased with the irradiation dose up to approximately 700 Gy of irradiation dose.

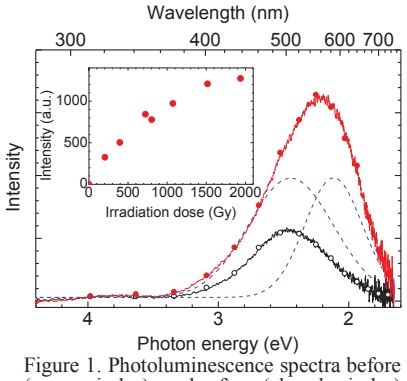

Figure 1. Photoluminescence spectra before (open circles) and after (closed circles) X-ray irradiation. Brocken lines are two components of the band after the irradiation. Inset: γ-ray dose dependence of the luminescence intensity.

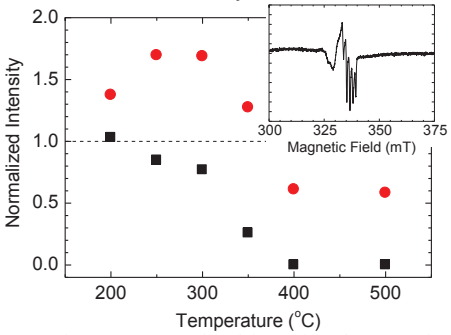

Figure 2. Normalized intensity changes of photoluminescence (circles) and ESR signal assigned to BOHC (squares) with heat treatment temperature after X-ray irradiation. Inset: ESR spectrum of Cu-SG after irradiation.

Figure 2 shows the variation in the photoluminescence intensity with heat treatments for the Cu-SG glass after the X-ray irradiation. The intensity increased with the heat treatments up to 300°C. This may be caused by the capture of electrons which are trapped at relatively stable sites, such as boron E' centers. Then the intensity gradually decreased with the heat treatments and returned to the initial intensity before the irradiation by the heat treatment at 500°C. The decrease in the intensity was consistent with that of the ESR signal intensity of the boron oxygen hole centers (BOHCs). This means that the decrease in the luminescence intensity was caused by the capture of holes which may be supplied from the BOHCs. The thermal stability of the photoluminescence up to 300°C and the prominent RPL in the Cu-SG are owing to the stability of the defects such as BOHC, which are generated in the glass by the exposure to radiation.

REFERENCE:

[1] H. Hashikawa, et al., *J. Am. Cer. Soc.*, **102**(4) (2019) 1642-1651.

CO4-11 Complex Structure of Ions Coordinated with Hydrophilic Polymer 21. Ionic Diffusion in Polymeric Structure Utilized by Polyiodide Ions. (2)

A. Kawaguchi , Y. Morimoto

IIRNS, Kyoto University

INTRODUCTION:

We have been investigating dynamical and interacted structures between iodine and polymers. Here, the term of "iodine" indicates not only simple I_2, but polyiodide ions (I_n^{m-}, *m, n*: integer, $n > 1$) as charged molecules, which suggest concealed potential and diverse availability. [1,2]

Experimentally, while polyiodide ions (and their counter-ions: ex. K^+ ion which exists within I_2-KI(aq)) are prepared as solutes in aqueous solution, both polyiodide ions as anion and counter-ion as cation can be simultaneously diffused into various polymeric matrix without deformation nor melting in macroscopic scale. Especially, diffusion of polyiodides and their counter ions ("iodine doping") into *hydrophilic* polymers advance drastically at room temperature. However, while preparation procedure can be easy operation with aqueous solutions at room temperature, there may be often observed unexpected and paradoxical behavior; for example, in PA6 (polyamide-6) matrices, "modified orientation of PA6 chain" or "diffusion and intercalation of doped elements into PA6 crystallite" can be observed. [3,4]

Additionally, polyiodide ions and counter ions behave as introducers for other following (posteriori diffused) ions and novel structure, including modification of original (non-doped) polymer itself. Or, in some cases, both paradoxical results, such as elimination vs. adsorption (dynamism by and among iodine), or softening vs. hardening (interaction between host polymers and "iodine"), or ordering vs. disordering (mobility of ions or polymer chains at each stage of hierarchic structure), can advance simultaneously.

Furthermore, even though interaction between polyiodide ions and *hydrophilic* polymers is explicit and drastic, there are many suggesting results observed in interaction between polyiodide ions and *hydrophobic* matrices which do not always indicate significant iodine doping quantitatively. [5]

Such interacted mobility of both guest ions and host polymer and complicated results in various polymers with polyiodide ions (or their diverse behavior in structure of host polymeric matrices) should be estimated considering "hierarchic structures" of polymer; it shall suggest potential generality penetrating polymeric structures, which are dominated by essential anisotropy destined through "polymer chains".

DISCUSSION:

Starting fundamentally, ionic diffusion as elemental transportation of solved solutes and diffusion through solvents requires two factors: independency of each ions and free mobilization.

Solving ions in microscopic scale means that molecules or ions are released from bulk solids in micro scale; otherwise, they turn back to aggregation. Such independency depends on affinity (chemical potential) between ions as solutes and solvents.

On the other hand, mobility of ions which are hydrated or solvated in (aqueous) solutions is guaranteed by dynamism of (hydrated or solvated) solvents. Generally, since solvent environments is implicitly regarded as (low) molecules in their liquid phase with activated mobility, solvation is hardly an obstacle against ionic mobility or diffusion. Then, affinity with solvent can be neglected as the obstacle for ionic mobility.

However, affinity with solvents is also viscosity for the solutes which may be the obstacle or a hurdle against mobility of the solutes. If so, affinity of ions as the solutes with the solvents and mobility of them in the solutes are opposed each other.

Then, affinity between "iodine" and polymers should be fixing the ions and should be the obstacles against mobility. Nevertheless, "iodine" or polyiodide ions indicate general affinity with polymeric matrices whereas their coordination also induces enhances mobility of (primary and following) doped ions or chain orientation in some cases (PA6). Here may be hints to explain logics of ionic diffusion through polymer in co-existence with "iodine". We suppose unneglectable suggestion applying generality of polymers behind the "iodine-doped" polymers, which may be regarded as particular cases. [to be continued]

ACKNOWLEDGMENTS: These results are researched with Dr. Gotoh (Shinshu Univ.) and his staff and are partially funded by NEDO.[6]

REFERENCES:

[1] patent. JPN-5444559 (2014).

[2] “Projects for Practical Use from Innovation” sponsored by NEDO (2007-2009).

[3] A. Kawaguchi, Polymer, **35**, 3797-3798. (1994).

[4] KAWAGUCHI Akio, et.al., SPring-8 User Exp. Rep. **5** (2000A), 354-354. (2000).

[5] A.Kawaguchi, Polym.Prep.Jpn., **62**,5116-5117. (2013).

CO4-12 Tritium release behavior from long term heated Li_2TiO_3 pebbles

K. Katayama, A. Ipponsugi, T. Hoshino[1], T. Matsumoto, and Y. Iinuma[2]

Interdisciplinary Graduate School of Engineering Sciences, Kyushu University
[1]Breeding Functional Materials Development Group, Fusion Research and Development Directorate, Quantum and Radiological Science and Technology
[2]Institute for Integrated Radiation and Nuclear Science, Kyoto University

INTRODUCTION: From the viewpoints of the feasibility and safety of the fuel cycle of a fusion reactor, it is important to understand tritium behavior in the blanket. Tritium release behavior from solid tritium breeding materials has been investigated by neutron irradiation in previous studies [1,2]. However, the influence of long-term high-temperature heating expected in a fusion DEMO reactor on tritium release are not sufficiently understood. In our previous study [3], it was observed that a certain amount of Li was evaporated from the Li_2TiO_3 pebbles by heating to a high temperature of 900 ºC and the grain size was increased by the sintering effect. These changes by heating pebbles may affect tritium behavior. In this study, Li_2TiO_3 pebbles were heated at 900 ºC in H_2/Ar flow for 720 hours at most and that was irradiated by neutrons in the Kyoto University Research Reactor. And then, tritium release behaviors from the pebbles by heating were observed in Kyushu University.

EXPERIMENTS: The sample pebbles of Li_2TiO_3 (Li/Ti ratio:2.00) were kindly provided by National Institutes for Quantum and Radiological Science and Technology. 4 samples were prepared by heated at 900 ºC in 1000 Pa H_2/Ar flow for 0, 72, 240, 720 hours, respectively. Each sample was packed in a quartz tube sealed under vacuum and neutron irradiated with the fluence of 1.65×10^{15} cm^{-2}. The irradiated samples were transported to Kyushu University and taken out from the quartz tube in a glove box filled with Ar gas. Each sample was packed in a quartz tube and heated to 1000 ºC in 1000 Pa H_2/Ar flow to enhance tritium release as HT by the isotope exchange reaction. The time variation of tritium concentration in the outlet gas was observed two ionization chambers, IC1 and IC2, which were connected in series. Water bubbler was installed between IC1 and IC2 to collect HTO. Total tritium concentration (HT + HTO) was monitored by IC1 and HT concentration was monitored by IC2.

RESULTS: Fig.1 compares the inner structure of Li_2TiO_3 pebbles as received and that heated at 900 ºC for 720 h. It seems that the particle size increased slightly, and the pores decreased. No considerable changes were seen in the structure after heating for 720 h. Fig.2 and Fig.3 show tritium release curves from Li_2TiO_3 pebbles as received and pre-heated for 720 h. For the sample heated for 720 h, the tritium release rate around 200-300 ºC became slightly slower, and the broad peak at the high temperature was not observed. It can be said that the influence of long-term heating on tritium behavior cannot be ignored.

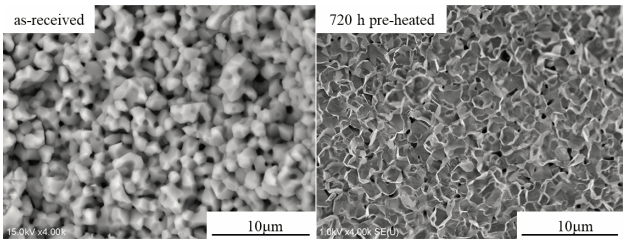

Fig. 1. SEM images inside pebble as received and 720 h pre-heated.

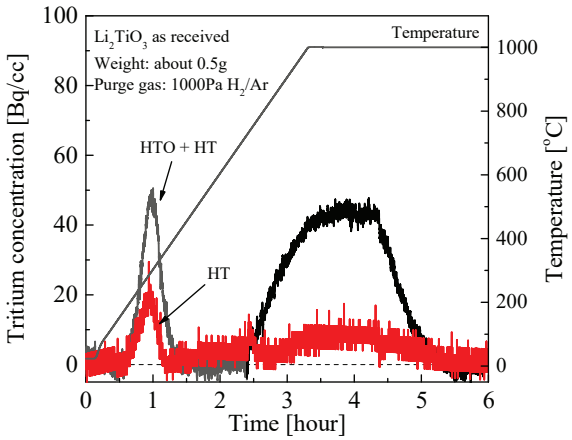

Fig. 2. Tritium release curve from Li_2TiO_3 pebbles as received.

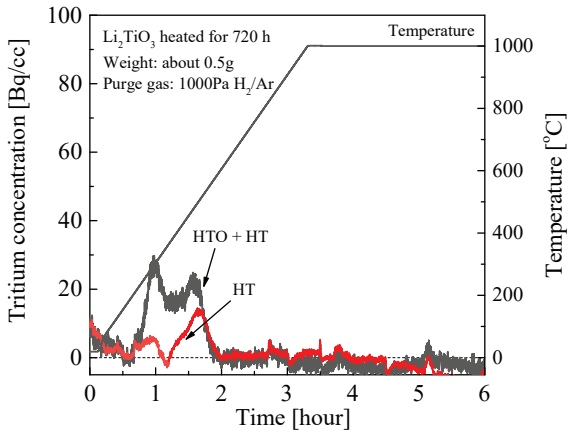

Fig. 3. Tritium release curve from Li_2TiO_3 pebbles pre-heated at 900 ºC for 720 h.

REFERENCES:

[1] T. Kinjyo *et al.*, Fusion Eng. Des. 83 (2008) 580-587.
[2] T. Hoshino *et al.*, Fusion Sci Technol. 67 (2015) 386-389.
[3] A. Ipponsugi *et al.*, Fusion Mater. Energy. 25 (2020) 100777.

CO4-13 Vacancy migration behavior in an $Al_{0.3}CoCrFeNi$ high entropy alloy

K. Sugita, M. Mizuno, H. Araki, A. Yabuuchi[1] and A. Kinomura[1]
Graduate School of Engineering, Osaka University
[1]*Institute for Integrated Radiation and Nuclear Science, Kyoto University*

INTRODUCTION: Alloy design has traditionally been done by selecting the base material and adding the appropriate elements to achieve the desired properties. In the last decade, a new type of multicomponent alloy called "high entropy alloys" containing equiatomic / near-equiatomic ratios of constituent elements was proposed by Yeh et al [1-3]. These alloys often exhibit simple solid solution structures at high temperatures due to the high constituent entropy of random solid solution mixtures. High entropy alloys have been reported to have promising properties for practical use, such as high strength, high fracture toughness, excellent oxidation resistance and corrosion resistance combined with ductility. A major factor in these properties is thought to be the kinetics of "sluggish diffusion". Therefore, the diffusion kinetics of high entropy alloys has been actively studied by diffusion logarithms and tracer diffusion methods, as the atomic diffusion in a multiprincipal element matrix has also been of interest. We have previously investigated the vacancy migration behavior during isochronous annealing after electron irradiation in CoCrFeMnNi high-entropy alloys and their subsystems and reported that the vacancy transfer energy does not change significantly with the number of constituent elements. In this study, we investigated the vacancy migration behavior in $Al_{0.3}CoCrFeNi$ high-entropy alloy and discussed the effect of Al addition on the vacancy migration behavior.

EXPERIMENTS: Arc melted ingots of an $Al_{0.3}CoCrFeNi$ alloy was purchased from Koujundo chemical laboratory (Japan). The ingots were homogenized at 1373K for 24 h in silica tubes under Ar atmosphere and were then machined into 10 × 10 × 0.5 mm plate pieces by electric discharge machining. The specimens were subjected to strain relief annealing at 1373K for 10 h and then rapidly cooled to prevent secondary phase precipitation and to stabilize single-phase FCC structures. The specimens in water flow were exposed to 8 MeV electron beam irradiation for 3 h in KURNS-LINAC. The irradiation damage was evaluated at (1.3 - 1.8) $\times 10^{-4}$ dpa. In order to investigate the thermal stability of vacancies, the electron irradiated specimens were subjected to the subsequent isochronal annealing at 373-673 K for 1 h.
Positron lifetime measurements were carried out by using a digital oscilloscope system with photomultiplier tubes mounted with BaF_2 scintillators, having a time resolution (FWHM) of 185 ps. The positron lifetime measurements require data acquisition for approximately 18 hours with a Na-22 positron source of 0.4 MBq activity in order to acquire 3 million counts in the positron lifetime spectrum. The measured spectra were analyzed using the programs RESOLUTION and POSITRONFIT Extended.

RESULTS: The mean positron lifetime after isochronal annealing of the electron irradiated samples is shown in Fig.1. The positron lifetime spectra of as-irradiated samples show a clear separation into two exponential components of positrons with a long lifetime of 185 ps. This indicates that a part of positrons is trapped by monovacancies or relatively small vacancy clusters introduced by during the electron irradiation. After the subsequent isochronal annealing, the mean positron lifetime is found to decrease sharply around 175°C. This can be attributed to the decrease in vacancy concentrations triggered by the free vacancy-migration. This result indicates that the vacancy migration energy in an $Al_{0.3}CoCrFeMnNi$ high-entropy alloy is lower than that in a CoCrFeNi alloy. This result is in contrast to the fact that the vacancy migration energies in an CoCrFeMnNi high-entropy alloy and its subsystems did not show any significant difference.

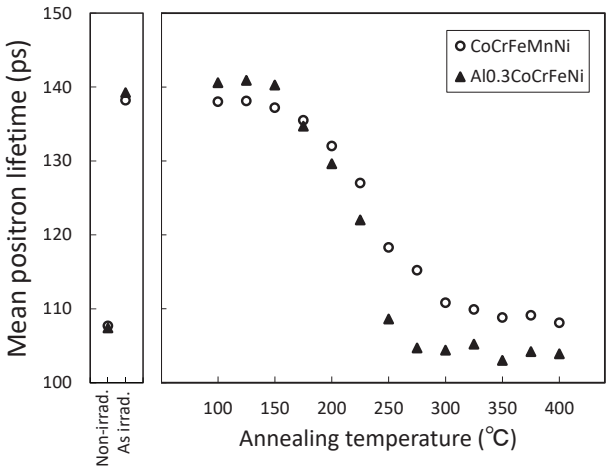

Fig. 1 Mean positron lifetime of electron irradiated CoCrFeMnNi and $Al_{0.3}CoCrFeNi$ high entropy alloys after isochronal annealing.

REFERENCES:
[1] C. Y. Hsu, J. W. Yeh, S. K. Chen, T. T. Shun: Metall. Mater. Trans. 35A, (2004), 1465.
[2] J. W. Yeh, S. K. Chen, S. J. Lin, J. Y. Gan, T. S. Chin, T. T. Shun, C. H. Tsau, S. Y. Chang: Adv. Eng. Mater. 6 (2004). 299.
[3] J. W. Yeh: Ann. Chim. Sci. Mat. 31, (2006), 633.

CO4-14 Construction of EO Sampling Detection System of Coherent Transition Radiation with Optical Cherenkov Radiation

T. Takahashi

Institute for Integrated Radiation and Nuclear Science, Kyoto University

INTRODUCTION: In recent years the THz-TDS has been widely used in the THz spectroscopy. The merit of the system is direct observation of the electric field. The conventional spectroscopic system using a bolometer can detect only the power of THz wave. Therefore the Kramers-Kronig analysis is necessary in order to calculate the optical constant. One of the detection system in the THz-TDS is the Electro-Optical (EO) sampling in which the induced birefringence by the Pockels effect is used. In the coherent THz radiation beamline [1] at the KURNS-LINAC, the bolometer has been used to detect the coherent radiation for a long time. In recent years, the application of the EO sampling to the detection of coherent transition radiation (CTR) in this beamline has been planned. Usually an ultrafast laser is used as a probe light in the THz-TDS. The strong point in this report is the usage of Cherenkov radiation in the visible region as a probe light. There is no jitter between CTR as the excitation light and Cherenkov radiation as the probe light. These are perfectly synchronized each other.

EXPERIMENTAL PROCEDURES: In AY2020, the beamtime of the linac was not enough to perform the experiment due to the covid-19 related confusion and some renovation work in the linac. In this report, only the experimental setup has been reported. The sub-THz radiation is the superposition of the forward CTR from the Ti-window and backward CTR from an aluminum-coated silica grass as shown in the Fig.1. The visible light for a probe of the EO-sampling is the Cherenkov radiation from a silica grass 5 mm thick. A ZnTe plate 1 mm thick is used as the EO device. The visible light is passed through a ZnTe plate, polarizer, a λ/4 retarder, and a Wollaston prism as shown in Fig.2. It is finally detected by a balanced detector which consists of two photo-diode detectors and amplified by a lock-in amplifier.

REFERENCES:

[1] T. Takahashi *et al.*, Rev. Sci. Instrum. **69** (1998) 3770.

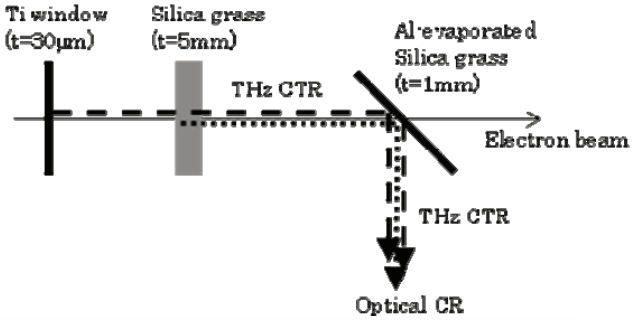

Fig.1. The schematic layout around the radiation source.

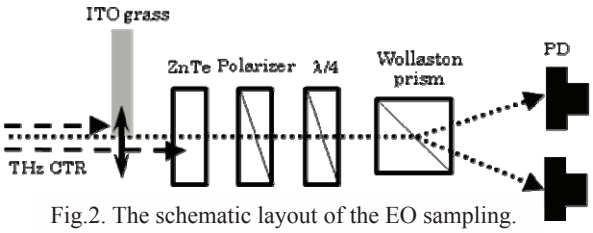

Fig.2. The schematic layout of the EO sampling.

CO4-15 Measurement of the Internal Pressure and Lifetime of Ultrafine Bubbles

D. Hayashi, M. Tanigaki[1]. Y. Ohkubo[1], A. Taniguchi[1], Y. Ueda[2], Y. Tokuda[3]

Graduate School of Science, Kyoto University
[1]KURNS
[2]Research Institute for Sustainable Humanosphere, Kyoto University
[3]Depertment of Education, Shiga University

INTRODUCTION: Ultrafine bubble (UFB), a bubble smaller than 1 μm, attracts so much attention because of its various applications, e.g., promoting the growth of fishery products. On the other hand, a fundamental study is not well extended because of the difficulty in the optical observation due to its smaller diameter than the wavelength of radiant-ray. Basic physical quantities of UFB are not investigated such as inner pressure, temperature, and lifetime.

Yamakura succeeded in measuring the pressure of UFB directly by the angular correlation measurement [2] based on the dependence of the anisotropy of cascade γ-rays of ^{125}I towards carrier-gas pressure [3].

In this paper, the extended studies of UFB by using the angular correlation measurement on the internal pressure and lifetime of UFB are introduced.

EXPERIMENTS: The pure water containing UFB of natural Xe gas with an average diameter of 100 nm was generated via the pressurized dissolution method. 4.0 ml of UFB water and saturated solution of natural Xe were separately packed to 4.5 ml polypropylene tubes and irradiated by thermal neutrons with the total dose of 6.9×10^{16} n/cm^2 at the slant exposure tube of Kyoto University Research Reactor (KUR) to activate ^{125}Xe through the reaction of ^{124}Xe (n, γ) ^{125}Xe. A different pair of samples was irradiated every few days to evaluate the time dependence of the remaining Xe in the samples. γ-γ cascades of 55 - 188 keV from ^{125}I obtained as the decay product of ^{125}Xe were detected by a CdZnTe detector (CZT) and one of two BaF_2 detectors. These two BaF_2 detectors are placed at the fixed angle of 90°, and a CZT on a turntable moves around the sample tube. With this configuration, the angular correlations of both 90°-θ and 180°+θ are measured at the same time. The correlation function of γ-γ cascade under the existence of hyperfine interaction is given as,

$$W(\theta) = 1 + A_{22}\overline{G_{22}(\infty)}P_2(\cos\theta)$$

where A_{22} is a constant of angular correlation, $\overline{G_{22}(\infty)}$ is a perturbed constant and the attenuation factor caused by hyperfine interactions.

RESULTS AND DISCUSSION: $A_{22}\overline{G_{22}(\infty)}$ for 55-188 keV cascade in ^{125}I was determined to be $+0.088 \pm 0.012$ from the obtained angular correlation (Fig.1). The pressure dependence of $A_{22}\overline{G_{22}(\infty)}$ for the 203 keV state in ^{127}I in Xe gas was well studied by Berek [3]. The result of ^{127}I can be converted to that of ^{125}I by simply applying the A_{22} for these states. From the obtained pressure dependence of $A_{22}\overline{G_{22}(\infty)}$, the internal pressure of UFB is tentatively determined to be $(4.15 \pm 0.67) \times 10^5$ Pa. The present result coincides with the result of Yamakura, $3.4^{+2.3}_{-1.3} \times 10^5$ Pa.

The time dependences of γ-γ cascades for both Xe-UFB samples and saturated Xe solution showed similar trends (Fig.2), and the $A_{22}\overline{G_{22}(\infty)}$ of saturated Xe solution corresponds to that of Xe-UFB. These results strongly imply the existence of Xe-UFB in the samples of saturated Xe solution. Terasaka recently reported the production of Xe-UFB by vibration or pressurization/depressurization of aqueous solutions of the gas [4]. Xe-UFB were possibly produced in the present experiment during the sample preparation or the transportation. Therefore, the lifetime of UFB is tentatively determined to be $(4.5 \pm 3.2) \times 10^2$ h from both time spectra. Additional lifetime measurements in a longer time span are expected.

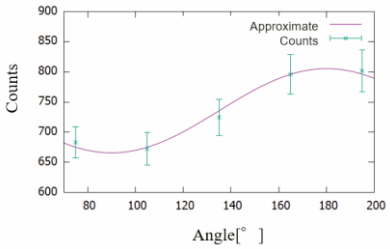

Fig.1. A typical anisotropy of the angle composed of the two 55-188keV cascades from ^{125}I in ^{125}Xe-gas.

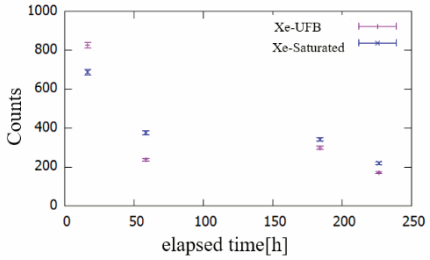

Fig.2. The time dependence of the 55-188keV cascade events of ^{125}I.

REFERENCES:

[1] J.G.HAn et.al, 'Lomg-term stability of hydrogen nanobubble fuel', Fuel 158 (2015) 399–404.
[2] T.Yamakura, Master Thesis 2018.
[3] U.Berek et al., Phys. Lett. 53A (1975) 251.
[4] K.Terasaka et al, Japanese J of Multiphase Flow, 10.3811/jjmf.2020.030.

R2081

CO4-16 Porosity Measurements of Sintered-Silver Bonding Plates

K. Wakamoto[1], T. Otsuka[1], K. Nakahara[1], A. Yabuuchi[2] and A. Kinomura[2]
[1]*Power Device R&D Department, ROHM Co., Ltd.*
[2]*Institute for Integrated Radiation and Nuclear Science, Kyoto University*

INTRODUCTION: Sintered silver has attracted much attention as a die-attach material for the power electronics, owing to its high heat dissipation capability [1]. On the other hand, the coefficient of thermal expansion (CTE) inevitably does not match each other of the materials used in a power system. Thus the heat-cycle oriented mechanical stresses deteriorate die-attach materials, and therefore the mechanical properties of sintered silver impinge on the reliability of electricity systems.

However, nobody can predict how long sintered silver sustains, because the material is porous and its mechanical properties heavily depends on how porous it is. Accordingly, the research is highly demanded to measure the porosity.

The porosity rate (p) of sintered silver is reported by some papers [2-3], where p is measured by using cross sectional scanning electron microscopy (SEM). These studies focus only on estimates the μm-order pores of sintered silver materials, not nm-order pores such as crystalline defects. Positron lifetime spectroscopy has advantages for this purpose. In this study, therefore, the authors evaluated nanometer-order pore sizes embedded in sintered silver with various p's by measuring the positron lifetime of the bulk material.

EXPERIMENTS: The fabrication process of sintered silver films is described as follows. Paste including silver nm-particles was stencil printed on a metal plate, and the containing organic solvent was dried at 140ºC for 1 h. These dried films were sintered at 200 - 300 ºC for 10 min with uniaxial press via a carbon buffer sheet with 0.5 – 120 MPa pressure. The film shape was 5 mm square and 50-μm thick. Positron annihilation lifetime spectroscopy was performed to evaluate bulk lifetimes of the samples by using a ^{22}Na source sealed with 12.5 μm Kapton foils. Four sample plates were stacked and measured together to stop all the positrons from the source inside the sample. The measured samples are summarized in Table I.

Table I Summary of the measured specimens.

Set	Sample	Sintering temp. (ºC)	Pressure (MPa)	Sample size
1	B,C,D	300	60,10,5	5mm square and 50-μm thick
2	A,B,C,D	300	120,80, 30,0.5	
3	E,F,G	300,240, 200	30	

The spectrometer consists of two scintillation gamma-ray detectors with BF_2 crystals and a spectrometer based on digital circuits. Total counts for each measurement were approximately 10^6 counts.

RESULTS: The data from the first and second sample sets to investigate pressure dependence was analyzed as follows. Measured lifetime spectra were decomposed into three components as shown in Fig. 1. It should be noted that the second lifetime was fixed to the previously reported value of dislocations in Ag (0.2 ns). The intensity of the second lifetime component changed in the range of 0.5 – 10 MPa, while the intensity of the third lifetime component corresponding to vacancy clusters were almost constant. Average lifetimes calculated from lifetime and intensity values were stable in the range of 0.20 – 0.23 ns (not shown) for all the samples. In previous studies using secondary electron microscopy (SEM), the porosity of the samples significantly changed depending formation pressure in the same range. The result of this study suggests that the information obtained from the positron measurements is clearly different from that obtained by the SEM observation.

In summary, nanometer-order porosity of sintered Ag plates was characterized as a function of formation pressure and temperature by conventional positron annihilation lifetime spectroscopy. The intensity of the second lifetime component corresponding to dislocations changed depending on formation pressure, while the average lifetime was almost constant.

REFERENCES:

[1] KIM S. SIOW, Journal of ELECTRONIC MATERIALS., **43** (2014) 947-961.
[2] T. Yousseff *et al*., Microelectronics Reliability., **55** (2015) 1997-2002.
[3] M. Takesue *et al*., Proc. PCIM., (2018) 148.

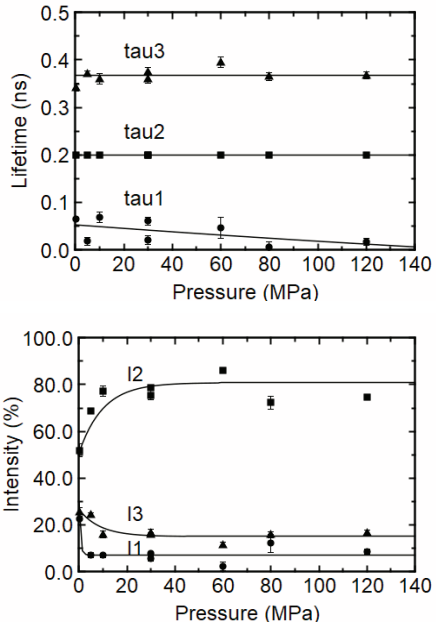

Fig. 1 Lifetimes and their intensities of the samples.

CO4-17 Demagnetization Measurement of Permanent Magnet Materials Against Neutrons Irradiation

Y. Fuwa[1], Y. Iwashita[2], Y. Kuriyama[3] and K. Takamiya[3]

[1]*J-PARC Center, Japan Atomic Energy Agency*
[2]*Insistute for Chemical Research, Kyoto University*
[3]*Institute for Integrated Radiation and Nuclear Science, Kyoto University*

INTRODUCTION: Permanent magnets are essential materials for particle accelerator components such as beam optical devices, insertion devices, and so on. In order to estimate the lifetime of the devices in a high-radiation environment, the demagnetization effects of permanent magnet materials were measured using Kyoto University Research Reactor (KUR). While rare earth magnets, such as NdFeB and SmCo, are known to have radiation demagnetization [1], there is not enough information for ferrite magnets, which are economical but have less remanent field strength. Furthermore, the demagnetization effect of NdFeB magnets is relatively wide fluctuations in the previous research. In order to acquire more precise insight into the demagnetization effect of permanent magnetic materials, we carried out a systematic experiment for measuring the demagnetization rate of the materials.

EXPERIMENTS: Samples for our experiments were anisotropic ferrite magnets, NdFeB magnets, and SmCo magnets. The shape of the samples was cylindrical with 5 mm diameter and 1 mm length that have easy-axis parallel to the cylinder axis.

We compared the magnetic field strength before and after the irradiations. In the measurement, Since the measurement using the Hall probe was sensitive to the positioning error of magnets, another measurement method was developed. In this method, the small magnet samples were rotated in a coil and the amplitude of the induced voltage was taken. This method is less sensitive to positioning errors.

The irradiation times were up to 4 hours at 1 MW operation (for Pn), 46 hours 1 MW operation and 6 hours at 5 MW operation (for HYD), and 4 weeks (for Long term irradiation plug). In these three irradiation conditions, estimated values of thermal neutron fluence on the samples are 7.0 x 10^{16} [n/cm^2], 5.7 x 10^{18} [n/cm^2] and 8.6 x 10^{18} [n/cm^2], respectively. After the residual radioactivity of the magnet and capsule decayed sufficiently, we took out the magnet samples from the capsule and measured the magnetic field.

RESULTS: For the results of NdFeB magnets, which have the highest residual magnetic field among the permanent magnet materials, the demagnetization rate leaches down to 80% with the neutron irradiation dose of 8.8 x 10^{14} [n/cm^2]. In this dose region, no demagnetization effects were detected for SmCo and ferrite magnets. SmCo magnets indicated no demagnetization effect up to 7.0 x 10^{16} [n/cm^2]. For the ferrite magnets, Fig. 1 shows the ratios of the magnetic field strength before and after the irradiation. The error bars show the standard deviations of measured data for each magnet. The broken vertical green line in Fig. 1 denotes the neutron dose at which radiation demagnetization becomes significant for NdFeB magnets as a comparison. According to the data taken so far, the characteristic radiation demagnetization dose is estimated at about 1.4 x 10^{20} [n/cm^2]. Because of the regression function form, the data points at fewer radiations have almost no effect on the fitting result. The magnetization will be degraded to half at a dose of about 1 x 10^{20} [n/cm^2].

PERSPECTICVE: The radiation hardness level of ferrite magnets close to those for SmCo magnets is important information for communities handling radiations. The ferrite magnets would be widely used in such applications. In our experiments, irradiation of ferrite magnets with 8 weeks and 12 weeks was performed. Since residual radioactivity was high for magnetization measurements, the measurement will be performed in 2021 after the radioactivity decays sufficiently. The results will show more information for the demagnetization of ferrite magnets.

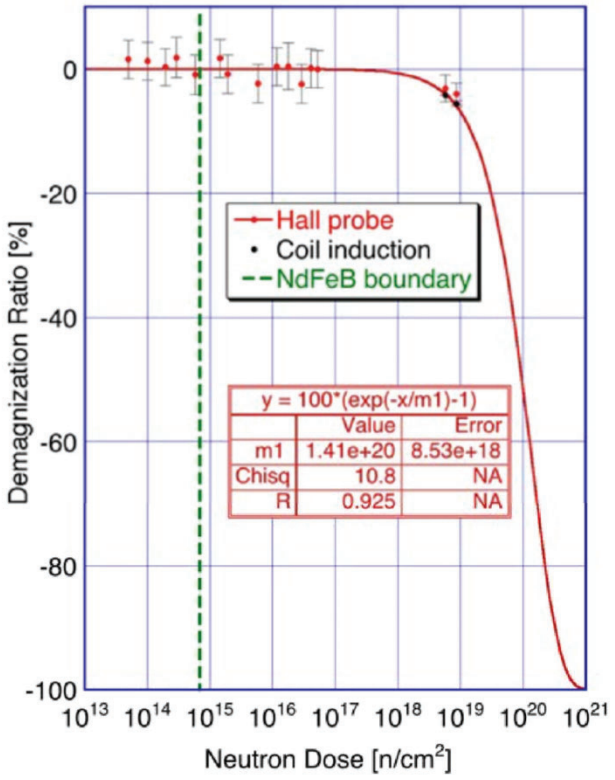

Fig. 1. Ratio of radiation demagnetization of ferrite permanent magnet.

REFERENCES:

[1] X. -M. Marechal, T. Bizen, Y. Asano, H. Kitamura, Proceedings of EPAC, Edinburgh, Scotland, 2006.

CO4-18 Neutron scattering study on microstructure of vitrified radioactive wastes

K. Kaneko, R. Motokawa, Y. Ohba, K. Mori[1], R. Oku-mura[1]

Materials Sciences Research Center, Japan Atomic Energy Agency
[1]Institute for Integrated Radiation and Nuclear Science, Kyoto University

INTRODUCTION:

The vitrification technique is used to immobilize high-level radioactive liquid wastes, which are yielded during reprocessing of nuclear fuels[1]. The high-level wastes are mixed with melted borosilicate glass, that results in forming an oxide. Among the constituents, molybdate tends to precipitate, that cause lowering of durability[2]. The segregation of platinoids is also problematic on fabrication[3]. In order to realize a long-term stability, deep understanding of the vitrification process becomes important.

Neutron diffraction is powerful probe to study structures of glass as it can access to high-Q range. In addition, its high transmission allows to investigate the vitrified waste as it is, namely, without crashing into powder required for x-ray. The latter could be essential to obtain an actual form of the waste. On the other hand, one of difficulties of neutron scattering arises from the fact that one of main constituents, boron, is strong neutron absorber. To avoid this issue, we prepared sample using ^{11}B enriched boron, and succeeded to observe neutron scattering pattern from the borosilicate glass without wastes. We extended the study for the sample with simulated wastes.

EXPERIMENTS:

The borosilicate glass with and without simulated radioactive wastes were prepared with an enriched ^{11}B, and to have cylindrical form with diameters for 5 mm and 10 mm, respectively.

Neutron diffraction experiments were performed on the versatile compact diffractometer installed at the B-3 beam port. Neutrons with a wavelength of 1 Å are provided by a Cu monochromator. An array of the ^{3}He detectors which covers 25˚ in the scattering angle enables efficient measurements.

RESULTS:

Figure 1 shows neutron transmission images of the borosilicate glass with and without simulated radioactive waste measured on the B-3. Whereas the borosilicate glass itself has sufficient transmission over 85 % as in Fig.1(a), almost no neutron can pass through the sample with simulated waste (Fig. 1(b)). By carefully check detailed composition, we identified that the simulated waste contains small fraction of Gd, being known as one of highest neutron absorber. To suppress absorption with keeping chemical characteristics, we replace Gd_2O_3 by La_2O_3. This substitution succeeded to increase transmission over 48 %. Neutron scattering pattern for this simulated waste glass sample is plotted in Fig. 2, together with the same borosilicate glass without wastes. The clear scattering patterns are successfully obtained for both samples. In addition, the data allow to identify that the mixing of waste gives rise to peak shifts and broadening from the raw glass, as clearly seen for peaks around 15˚ and 50˚. This result confirms that a part of wastes is incorporated into a network structure of the glass.

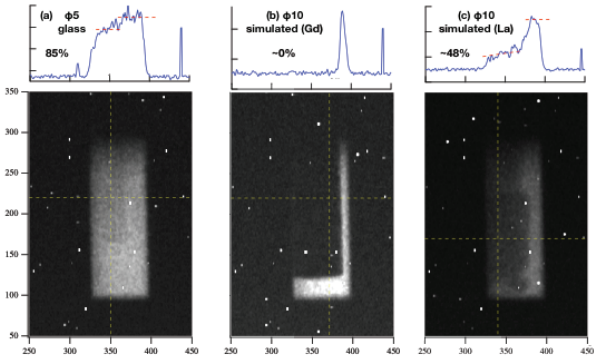

Fig. 1. Neutron transmission image of the borosilicate glass (a) without and (b,c) with simulated radioactive wastes. One of the constituents of simulated waste, Gd_2O_3, in the sample (b) is replaced by La_2O_3 in the sample (c) to avoid strong neutron absorption of Gd.

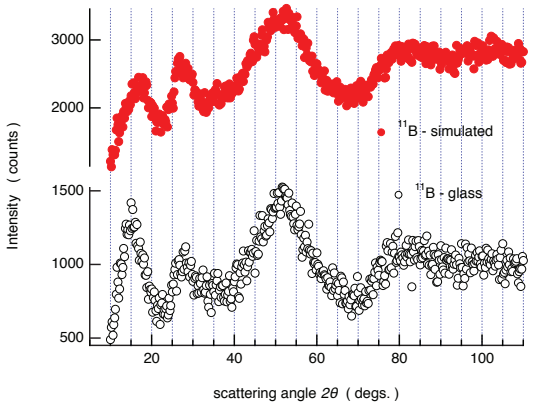

Fig. 2 Neutron scattering pattern of the borosilicate glass with and without simulated radioactive wastes.

The present result proves that neutron scattering can offer further insights into the structure of the borosilicate glass and impact of wastes for it. Further study on the simulated waste with different compositions and fabrication conditions will enable us to optimize the vitrification of the radioactive waste.

REFERENCES:

[1] G. Roth, S. Weisenburger, Nucl. Eng. Des. **202**, 197e207 (2000).
[2] S. Morgan *et al.*, Mater. Res. Soc. Symp. Proc. **807**, 151e156 (2003).
[3] H. Mitamura *et al.*, Nucl. Chem. Waste Maenag. **4**, 245e251 (1983).

CO4-19 Research on Polymer Composite Materials Containing Ion-implanted Metal Nanoparticles Using a Slow Positron Beam

Y. Kobayashi[1], T. Kavetskyy[2], A. Yabuuchi[3] and A. Kinomura[3]

[1]*Waseda Research Institute for Science and Engineering, Waseda University*
[2]*Department of Biology and Chemistry, Drohobych Ivan Franko State Pedagogical University*
[3]*Institute for Integrated Radiation and Nuclear Science (KURNS), Kyoto University*

INTRODUCTION: Controlling the size of nanoparticles (NPs) in a polymer matrix is important for fabrication of nanocomposites with foreseen properties for their applications in nanophotonics, electronics, biomedicine, etc.. In particular, the nanocomposites containing Ag-NPs dispersed in the polymer matrix by low-energy (< 100 keV) ion implantation with high ion fluences (> 10^{16} ions/cm^2) can be used for fabrication of plasmonic waveguides [1] and diffraction gratings as well as for anti-microbial applications.

Positron annihilation spectroscopy (PAS) employing a variable-energy slow positron beam is a versatile technique for characterization of defects in thin films, allowing depth-profiles from tens of nanometers up to several micrometers. This technique has been successfully utilized as a major experimental tool to understand carbon nanostructures kinetics during high fluence B ion implantation into polymethylmethacrylate (B:PMMA) [2].

In our previous studies [2,3], usage of both Doppler broadening and positron lifetime methods in combination with other tools (e.g. UV-Vis absorption and Raman spectroscopy) allowed successful verification of the formation of carbon nanostructures in B:PMMA samples. A key point for such conclusion in the case of ion-implanted B:PMMA was positron annihilation lifetime spectroscopy (PALS) data at the positron energy corresponding to a depth of implanted range of the sample with maximum radiation damage, showing no *ortho*-positronium (*o*-Ps) yield at high ion fluences (> 10^{16} ions/cm^2); the same, there is no *o*-Ps yield in carbon based materials such as, for instance, fullerene C^{60} cage and carbon molecular sieve membranes. Thus, taken this *o*-Ps yield feature in carbon based materials into consideration, it is expected that similar important information should be obtained for investigating the ion-synthesized silver nanoparticles in polymer matrixes containing carbon clusters or carbon nanostructures formed upon ion bombardment.

EXPERIMENTS: The positron pulsing system of the KUR slow positron beam system have been developed for PALS of thin films or near-surface layers. It is confirmed that the pulsing system is effective for samples with relatively short positron lifetimes (τ < 1 ns) such as metals and semiconductors without o-Ps formation. In this study, we examine the validity of the PALS measurement system of the KUR slow positron beamline for samples with o-Ps components. Acceleration energies of 2 - 3 keV was used for PALS measurements.

RESULTS: Figure 1 shows the Kapton spectrum (closed circles) with simulated spectra (solid and broken lines) after background subtraction. The simulated spectra assumed two lifetime components with the Kapton lifetime and longer lifetimes (2, 5 and 10 ns with 10% intensity). One of the problems with PALS measurements in the KUR system is higher background signals. Indeed, unwanted satellite peaks originating from a radiofrequency-driven-buncher exist on the background signals with a period of the buncher signal as shown in Fig. 1. Such signals prevent appropriate o-Ps lifetime/intensity determination in PALS measurements. The simulated spectra in Fig. 1 suggest that relatively shorter o-Ps components (<5ns) are acceptable. But, for the longer o-Ps component, appropriate fitting or background-subtraction procedures are required. Figure 2 shows the lifetime spectrum for a polymer thin film for a trial measurement. In this case, an o-Ps component can be observed but its lifetime is sufficiently shorter to avoid the influence of the satellite peak.

In summary, the PALS measurement system of the KUR slow positron beamline was applied for polymer materials with long lifetime (o-Ps) components. The result suggested that the PALS system was effective for relatively shorter o-Ps components.

REFERENCES:

[1] T. Kavetskyy *et al*., Phys. Status Solidi C, **9** (2012) 2444-2447.
[2] T. Kavetskyy *et al*., J. Phys. Chem. B, **118** (2014) 4194-4200.
[3] T.S. Kavetskyy, A.L. Stepanov, in *Radiation Effects in Materials*, edited by W.A. Monteiro (InTech, Rijeka, 2016), p. 287-308.

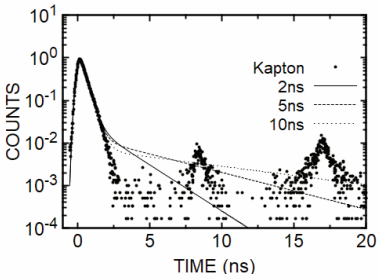

Fig. 1 Kapton spectrum and simulated spectra with long lifetime components.

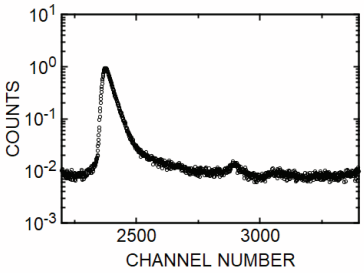

Fig. 2 Spectrum of the measured polymer film.

CO4-20 Study of resonant frequency change with irradiation dose of piezoelectric PZT element

M. Kobayashi, T. Miyachi, S. Takechi[1], Y. Morita[1], Reo Kunimatsu[2] and Ryo Sasaki[2]

Planetary Exploration Research Center, Chiba Institute of Technology
[1]Graduate School of Engineering, Osaka City University
[2]Department of Engineering, Osaka City University

INTRODUCTION: The aim of this research is to establish an inexpensive method for dosimetry in high dose environments. We consider the use of the change in piezoelectricity of piezoelectric elements due to irradiation for dosimetry in high dose environments. For this purpose, we have investigated the mechanism of radiation-induced change in piezoelectricity by experiments. As in the past, this year we conducted another experiment to investigate the change in piezoelectricity caused by electron beams.

In a previous experiment conducted at HIMAC/NIRS, we irradiated a piezoelectric PZT element with 400 MeV/n Xe particles and investigated the decrease in the electromechanical coupling coefficient k [1]. It was shown that the energy imparted was proportional to the decrease in the coupling coefficient of the irradiated PZT element.

In this study, we have conducted an experiment using electron beam to investigate the effect of electron beam on the decrease in the coupling coefficient of the irradiated PZT element at KUR/LINAC. As a result, it was found that the electromechanical coupling coefficients decreased linearly with the absorbed dose in electron irradiation, although the change was smaller than that in Xe irradiation. Even though the absorbed dose is the same, the change in the electromechanical coupling coefficient is more than one order of magnitude smaller for electron irradiation.

Over the past few years, we have been experimenting with improved and modified experimental setups in order to obtain more accurate values. We improved the alignment of the element installation and the air-cooling method to stabilize the element temperature, thereby stabilizing the accumulation of measured values. In addition, we measured the PZT temperature during irradiation and corrected the amount of change in k due to the temperature rise, which was measured separately using a thermostatic bath. With these measures, the variation of the piezoelectricity change was eliminated, and the piezoelectricity change due to electron beam irradiation could be measured accurately.

EXPERIMENTS: Although we found that the piezoelectricity (electromechanical coupling coefficient k) changes linearly with the amount of electron beam irradiation, there was an event where the value of k changed discontinuously before and during the experiment. Until last year, in order to measure k, we soldered a cable to the PZT device and connected it to the impedance analyzer. In other words, when the cable was soldered to the PZT device, the temperature of 200°C or higher was applied locally even for a short period of time, and we could not eliminate the possibility of k changing due to this. To solve this problem, we used a phosphor-bronze plate spring to fabricate an electrode to contact the cylindrical PZT device between them, and used it as an irradiation jig. As a result, the discontinuous change of k before and after the experiment was eliminated, and the change of k in response to the amount of electron irradiation could be investigated more accurately.

FUTURE PERSPECTIVE: Based on the results to date as described above, we are considering the following experiments to be conducted in the future.

(1) *Effect of PZT element shape*: In our previous experiments, we have used a cylindrical PZT element with a diameter of 18mm x t12mm. To calculate the electromechanical coupling coefficient *k, we used an* approximate equation that can be applied to a disk-shaped element (applicable to a diameter > 10 times the thickness), which is probably fine for the purpose of knowing the relative change, but may be problematic when discussing the validity of the approximate equation. Therefore, we would like to investigate the adaptability by using a PZT device with a shape that meets the conditions of the approximation formula (disk shape with diameter > 10 times the thickness).

(2) *Types of PZT elements (soft material, high temperature soft material, high temperature hard material)*: The PZT devices used in our experiments so far are so-called "soft materials" and have a relatively low Curie temperature. By investigating the characteristics of other types of PZT elements, we hope to elucidate the mechanism of piezoelectricity change by radiation irradiation and to apply it to radiation measurement devices.

(3) *Effects of Neutrons*: After electron irradiation, PZT elements radiate and emit characteristic gamma rays. This is the possibility that the PZT element loses its piezoelectricity due to inelastic scattering by neutrons or nuclear reaction by neutron capture. To consider this, we would like to measure the neutron flux during electron irradiation at the LINAC.

REFERENCES:

[1] S. Takechi et al., Japanese Journal of Applied Physics 60 038003 (2021)
[2] M. Kobayashi et al., Japanese Journal of Applied Physics 53, 066602 (2014).
[3] M. Kobayashi et al., Japanese Journal of Applied Physics 52, 126604 (2013).

R2110

CO4-21

Tritium recovery behavior for tritium breeder of Li_4SiO_4 – Li_2TiO_3 mixture material

Y. Oya[1,2], S. Hirata[2] K. Ashizawa[2], Y. Koyama[2], F. Sun[1], Y. Iinuma[3]

[1]*Faculty of Science, Shizuoka University*
[2]*Graduate School of Integrated Science and Technology, Shizuoka University*
[3]*Institute for Integrated Radiation and Nuclear Sci-ence, Kyoto University*

INTRODUCTION: In the fusion reactor blanket, tritium is produced by (n, α) reaction with lithium. Solid lithium ceramic is considered as one of candidates for blanket materials. Especially, Li_2TiO_3 and Li_4SiO_4 are regarded as one of the promising solid breeder candidates due to relatively higher chemical stability and higher lithium atom density. For Li_4SiO_4, lithium atomic density is higher than that for Li_2TiO_3, but its chemical stability is not good. Recently, Li_4SiO_4-Li_2TiO_3 mixture materials are proposed as advanced candidates to compensate for shortcoming, and several mechanical properties have been evaluated. However, the tritium recovery performance was not still understood. In this study, Li_4SiO_4-Li_2TiO_3 mixture materials with various phase ratios were used and their tritium desorption behavior after neutron irradiation was evaluated using tritium thermal desorption spectroscopy (TDS).

EXPERIMENTS: Two kinds of samples with different phase ratios, namely Li_4SiO_4-Li_2TiO_3 (sample 1) and Li_4SiO_4-$2Li_2TiO_3$ (sample 2 and sample 3), were prepared. These materials were pebble samples that dominator 6 mm or less before neutron irradiation. These materials were installed into Kyoto University Research reactor (KUR), and the neutron irradiation was performed with the fluence of ~ 8.0×10^{15} n cm^{-2} or 8.0×10^{16} n cm^{-2}. Only sample 2 was irradiated with higher fluence of 8.0×10^{16} n cm^{-2}. Thereafter, tritium TDS measurement was conducted from R.T. to 1113 K with the heating rates of 5 - 20 K min^{-1}. The amount of desorbed tritium was evaluated by a liquid scintillation counter.

RESULTS AND DISCUSSION: Most of tritium was released as a water-form. Fig. 1 shows TDS spectra for 10 K min^{-1}. Tritium TDS spectra for Li_4SiO_4-$2Li_2TiO_3$ samples with different neutron fluence showed that the release temperature for sample 2 was located at around 520 K and that for sample 3 was around 630 K. Li_4SiO_4-$2Li_2TiO_3$ samples had single tritium desorption stage, and its activation energy was evaluated to be 0.44 - 0.47 eV. This result was almost consistent with that for Li_2TiO_3 sample.[1] The rate-determination step for tritium recovery can be explained by the diffusion-limited process. Li_4SiO_4-Li_2TiO_3 had multi-tritium desorption stages. The activation energy of the most significant tritium desorption peak was estimated to be 0.72 eV. The release temperature for mixture materials was lower than that for Li_2TiO_3 or Li_4SiO_4. The amount of tritium that Li_4SiO_4-$2Li_2TiO_3$ samples released was 1.40 MBq g^{-1} and 1.99 MBq g^{-1}. Lower fluence sample released more tritium than higher fluence sample due to crack-up of samples during neutron irradiation. The amount of tritium for Li_4SiO_4-Li_2TiO_3 sample was 0.79 MBq g^{-1}. Lower activation energy and amount of desorbed tritium, Li_4SiO_4-$2Li_2TiO_3$ has lower activation energy for tritium release, and it will be quite suitable for tritium recovery at lower temperature.

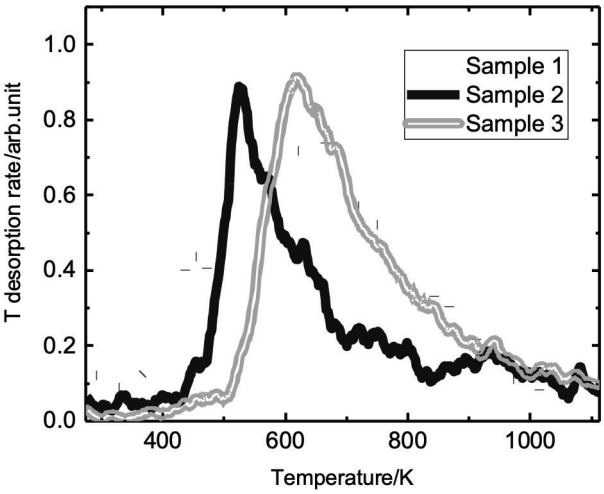

Fig. 1. Tritium TDS spectra for Li_4SiO_4-Li_2TiO_3 (sample 1) and Li_4SiO_4-$2Li_2TiO_3$ (sample 2 and sample 3) with the heating late of 10 K min^{-1}.

REFERENCES:

[1] Qilai Zhou et al., J. Nucl. Mater. 522 (2019) 286-293.

R2115

CO4-22 Formation of radiation defects on tungsten and their influence on effect of hydrogen isotope retention

K. Tokunaga, M. Matsuyama[1], M. Hasegawa, K. Nakamura and Q. Xu[2]

Research Institute for Applied Mechanics, Khushu University
[1]Hydrogen Isotope Research Center, University of Toyama
[2]Institute for Integrated Radiation and Nuclear Science, Kyoto University

INTRODUCTION: It is of a great importance to clarify phenomena of implantation, retention, diffusion and permeation of tritium (T) on surface of the armor materials of the first wall/blanket and the divertor on fusion device from a viewpoint of precise control of fuel particles, reduction of tritium inventory and safe waste management of materials contaminated with tritium. Refractory metals such as tungsten (W) is potential candidate for the armor of the first wall and the divertor plate of the fusion reactor because of its low erosion yield and good thermal properties. The armor material will be subjected to heavy thermal loads in the steady state or transient mode combined with high energy neutron irradiation that will cause serious material degradation. In addition, high energy runaway electrons would bombard the armor materials along the equatorial plane in fusion device. It is considered that these cause radiation damage and enhance tritium retention. In the present works, T exposure experiments have been carried out on W samples which were irradiated by high energy electrons to investigate effects of high energy electrons irradiation on microstructure and tritium retention of W. In this fiscal year, pure W and recrystallized W were irradiated by high energy electron beam. Before and after that, positron annihilation experiment was carried out to identify the radiation defect. In addition, EBSD（Electron Back Scatter Diffraction Patterns）analyses has been carried out on the specimens before and after the electrons irradiation. Tritium exposure experiments have been carried out using a tritium (T) exposure device.

EXPERIMENTS: W samples used were ITER specification W (ALMT-grade) (SR-W) and its recrystallized W (RC-W). The SR-W was fabricated via a powder metallurgical route including cold isostatic pressing, sintering, hot rolling, and heat treating to relieve the residual stresses. Some of the machined SR specimens were subjected to a full recrystallization treatment at 2000 ºC for 1 hr in vacuum. Sizes of the specimens were 10 mm x 10 mm x 1mm (10 mm x 10 mm : ND-TD). The surface of the both samples were polished to be mirrored. High energy electrons irradiation has been carried out using LINAC in Institute for Integrated Radiation and Nuclear Science, Kyoto University. An peak energy of electron irradiated was 8 MeV and DPA was 5.8 x 10^{-3}. Temperature during the irradiation was measured by thermocouples which was contacted with a backside of the W samples. Before and after that, positron annihilation experiment was carried out to identify the radiation defect. In addi-tion, EBSD（Electron Back Scatter Diffraction Patterns）analyses has been carried out on the specimens before and after the electrons irradiation. T exposure experiments have been carried out using a T exposure device in University of Toyama. Pressure of the T gas was 1.3 kPa and T exposure was kept for 4 h. T concentration in the gas was about 5 %. After the exposure to T gas, T amount retained in surface layers of the sample was evaluated by β-ray-induced X-ray spectrometry (BIXS) and imaging plate (IP) measurements.

RESULTS: Figure 1 shows X-ray spectra observed for the SR-W(a) and RC-W(b) which were not irradiated by the high energy electrons. Temperature of T exposure is 350ºC. In the case of SR-W, WM_α, ArK_α, WL_α and bremsstrahlung X-rays are detected. These results indicate that T exists deeper area than that of RC-W. This is considered that T traps with the internal defects in the SR-W. T exposure on the samples after the electron irradiation is undergoing.

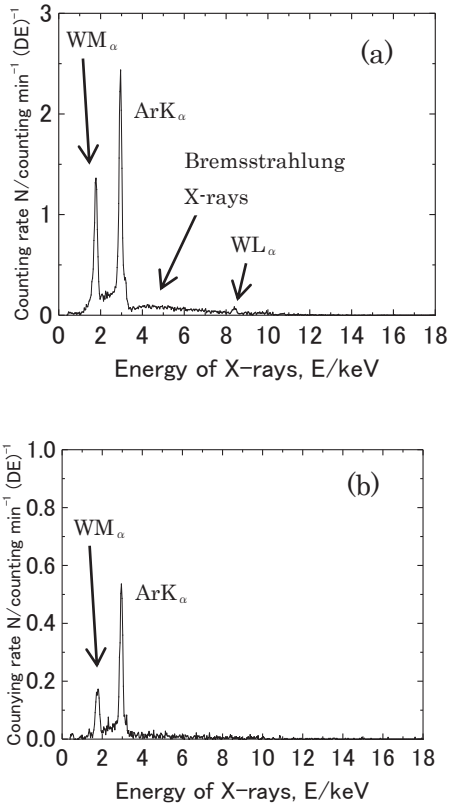

Fig. 1. X-ray spectra for SR-W(a) and RC-W(b) by BIXS.

CO4-23 SAXS Analysis of Heat Denaturation of Soybean Proteins

N. Sato, A. Okuda, K. Morishima, R. Inoue, R. Urade, and M. Sugiyama

Institute for Integrated Radiation and Nuclear Science, Kyoto University

INTRODUCTION: Soybean has long been served as dietary food because of its rich nutritional ingredients, especially proteins. Various kinds of soybean food products such as *miso*, *tofu*, and *tofu* skin (*yuba*) have been produced and eaten as well as unprocessed soybeans themselves. Recently soybean proteins are utilized as soy protein isolate (SPI) in food industries to be added in other food products to improve their physical properties, such as water retention, binding property, and gelling property. Soybeans also play a crucial role in producing mimic meat for vegetarians and vegans. Since soybeans contain an exceptionally high amount of protein for a plant, they are regarded as the most proper alternatives for animal meat. The physical properties of those food products are subject to those of soybean proteins. Therefore it is important to understand the nature of soybean proteins to produce high quality not only soybean food products but also SPI-containing food products, and mimic meat.

Physical properties of protein-containing food products have close relationship with their assembly structure of their component protein molecules in the nanometer scale. In general, raw materials of foods are finely ground, dispersed in water, and then heated. Therefore structural changes of the proteins in hydrates or solutions induced by heat are a significant issue both from scientific and industrial points of view. However, the nanostructural analysis of food products is often difficult owing to their disordered nature, opacity, and aggregation. Small-angle X-ray and neutron scattering (SAXS, SANS) are powerful tools for investigating nanostructure of those kinds of materials. A great number of SAXS and SANS researches has been carried out until now for so-called soft matters, such as rubber, colloids, and polymer gels. By taking advantages of their feature, we have been focusing on the nanostructural analyses of plant food proteins of wheat and soybean by SAXS and SANS. One of our studies is regarding the structure of the assembly of wheat protein gliadins in a wide concentration range of water [1].

In the present study, we investigated thermal denaturation process of two major soybean proteins, β-conglycinin and glycinin, which have been conventionally referred to as 7S and 11S, respectively, according to their sedimentation coefficients determined by analytical ultracentrifugation. Structural changes induced by thermal treatment was investigated by SAXS as the treatment temperature changing was changed, and the difference of heat-resisting property between 7S and 11S was revealed under the various conditions of buffer solutions.

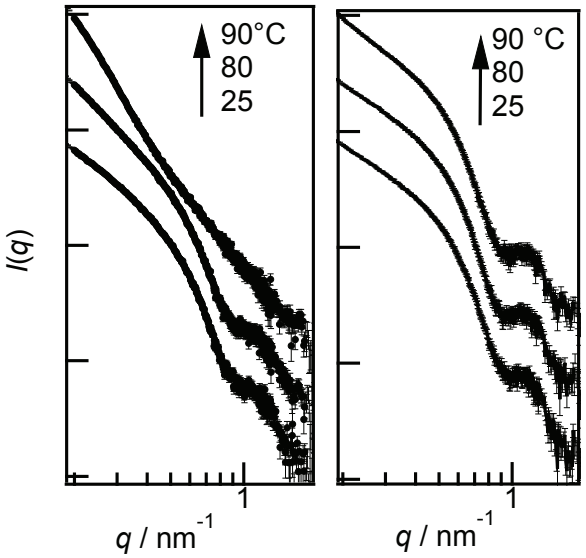

Fig. 1 SAXS profiles for 11S in KPi buffer solutions. NaCl concentration was 0 M(left) and 0.4 M (right).

EXPERIMENTS: Soybean proteins 7S and 11S were extracted from hexane-defatted powder of soybean cultivar "Enrei" under a reducing condition with 2-mercaptoethanol. Isoelectric precipitation was applied to isolation of each protein. By adjusting pH of the extract solutions, 11S and 7S was precipitated at pH 5.8 and pH 4.5, respectively. SAXS measurements were performed with a laboratory SAXS instrument (NANOPIX, Rigaku) installed at Institute for Integrated Radiation and Nuclear Science, Kyoto University. Each protein was dissolved as to be a concentration of 3% in a 35-mM potassium phosphate (KPi) buffer solution at pH 7.5 in presence of 0 or 0.4 M NaCl. The solutions were kept at a given temperature for 5 min and then cooled to 25°C. After that, they were put into aluminum cells and set for SAXS measurements. The wavelength of X-ray was 1.54 Å, the sample-to-detector distance was 1300 mm and the available q-range was 0.1 – 2.0 nm^{-1}.

RESULTS: The SAXS profiles for 7S and 11S showed a peak around 1.2 nm^{-1}, indicating trimer ring structure composed of three subunits of the protein. The peak was obvious for 7S and 11S both with and without NaCl, but became vague for 7S around 75°C. This fact shows that the ring structure of 7S is lost around this temperature due to denaturation of the protein. In contrast, as Figure 1 shows, the peak indicating ring structure remained until 80°C without NaCl, and even until 90°C in the presence of NaCl. This result demonstrates that 11S has higher structural stability than 7S against high temperature, and also that NaCl has strengthening effect for reluctance thermal denaturation.

REFERENCES:

[1] N. Sato *et al.*, *J. Agric. Food Sci.*, **63** (2015) 8715.

CO4-24 Study on HPLC Elution Behavior of Metallofullerenes Encapsulating Heavy Lanthanide Elements

K. Akiyama, K. Amekura, S. Nishimura, K. Ikeda[1], T. Kuroda and S. Kubuki

Graduate School of Science, Tokyo Metropolitan University
Department of Chemistry, Tokyo Metropolitan University

INTRODUCTION: Metallofullerene is well known as one of the clathrate compounds which incorporates metal atom inside fullerene cage [1]. The metallofullerenes encapsulating lanthanide element ($Ln@C_{2n}$, Ln: lanthanide atom, n > 30) have two or three charge transferred electrons on the fullerene surface and their electronic state are strongly affected by the number of the charge transferred electrons [1]. On the other hand, it is known that there is a slight difference in the High-Performance Liquid Chromatography (HPLC) retention time of $Ln@C_{82}$ metallofullerene including different Ln atom despite the same number of the charge transferred electron because the HPLC retention time of the fullerene species is strongly affected by the number of π electrons on the fullerene surface [2]. According to the chromatographic theory, HPLC retention time correlates with equilibrium constant *K* of the adsorption/desorption and also follows the van't Hoff equation [3]. From this correlation, the adsorption/desorption enthalpy can be obtained as the slope of the function $1/T$, which reciprocal of the temperature. Since the adsorption/desorption enthalpy is related to the parameters concerning about the electronic state of metallofullerenes such as the polarizability and the dipole moment, it is possible to obtain information about the electronic states of metallofullerenes by studying the temperature dependence of the retention time.
As mentioned above, it is found difference among HPLC retention time depending on the condition in HPLC development, such as temperature. Accordingly, it is necessary to perform the simultaneous multi-elemental analysis. However, since it is impossible to distinguish each metallofullerene by ordinal detection method for monitoring UV absorption, it is strongly required to employ for the radio chromatography in which γ-rays are monitored.
In this study, we tried to clarify the electronic properties of lanthanide in the fullerene cage affected on the multi-stage adsorption/desorption equilibrium in HPLC separation by the radio chromatography.

EXPERIMENTS: Purified $Tb@C_{82}$ metallofullerenes, which was produced by arc discharge method, was mixed with roughly purified C_{60} as a radical scavenger and then was sealed into polyethylene vials. This sample was irradiated by thermal neutrons at pneumatic irradiation facility of Pn-1 in KUR for 4 hours. After the irradiation, this sample was dissolved into toluene and mixed with each other. This toluene solution was injected into a HPLC column of COSMOSIL Buckyprep with the flow rate of 3.2 mL/min at -50 °C employed ethanol/water mixed solution (volume ratio of 80%/20%) with dry ice as a refrigerant. The eluate from the column were collected by every 1 minute from 30 min to 150 min and γ-rays emitted from each sample were measured by Ge detector.

RESULTS: Figure 1 shows the HPLC chromatogram monitored by UV absorption together with radio chromatogram of ^{160}Tb. The γ ray from ^{160}Tb was only observed in 114 min fraction. At the room temperature, HPLC elution peaks of $Ln@C_{82}$ are found around 60 min. $Tb@C_{82}$ is one of the species which has the largest HPLC retention time among each $Ln@C_{82}$ from our knowledge. It is expected that this tendency will not change even at lower temperature, this result is very important as a guide line for the future works.

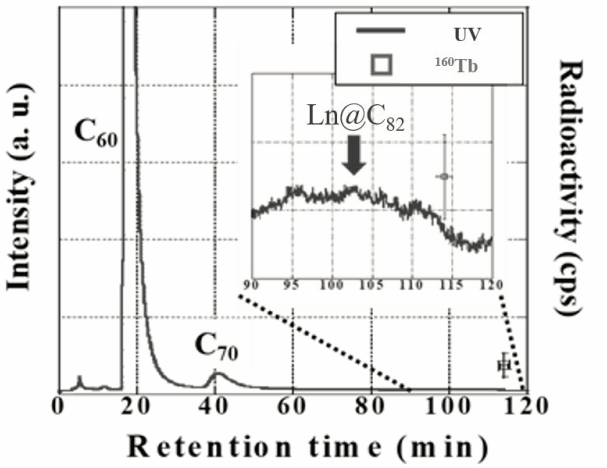

Fig. 1. HPLC chromatogram of fullerenes monitored by UV absorption together with radio-chromatogram monitored by γ-ray emitted from ^{160}Tb.

REFERENCES:
[1] H. Shinohara, Rep. Prog. Phys. **63** (2000) 843-892.
[2] D. Fuchs *et al.*, J. Phys. Chem. **100** (1996) 725-729.
[3] J. Cazes and R. P. W. Scott, in Chromatography Theory (Mercel Dekker, Inc., New York, 2002).

CO4-25 A study on destruction of cesium aluminosilicate compounds by gamma irradiation (2)

H. Ohashi, H. Umetsu, T. Saito[1]

Faculty of Symbiotic Systems Science, Fukushima University
[1]Institute for Integrated Radiation and Nuclear Science, Kyoto University

INTRODUCTION: Pollucite which is one of cesium aluminosilicate compounds have attracted attention as a final storage material of ^{134}Cs and ^{137}Cs. Pollucite is able to synthesized by hydrothermal method in low temperature below 300°C [1]. Pollucite has various properties that favor the immobilization of Cs ions.

However, the damage to the aluminosilicate framework by radiation decay is concerned because it contains ^{137}Cs. It has been reported that the effect of β-ray emission and nuclide conversion by β-decay of ^{137}Cs on aluminosilicate framework is minor [2, 3]. On the other hand, there are few reports of effects by gamma rays on pollucite framework. Therefore, we examined the effect of gamma radiation on the aluminosilicate framework of Pollucite. Pollucite samples were synthesized to investigate the effect of gamma irradiation.

EXPERIMENTS: Sodium aluminate, sodium metasilicate and cesium chloride were dissolved in sodium hydroxide solution. The solution was placed in a Teflon inner cylinder pressure container. Pollucite was synthesized by hydrothermal method, holding the container at 180°C for 48 hours. The resulting precipitate was washed. Thereafter, each solid was collected by filtration and dried at 110 °C for 12 hours or more.

The powder samples were characterized by XRD, and gamma-irradiated at 0 and 100 kGy by ^{60}Co source. The 7 days leaching test by PCT-A method [4] was carried out to evaluate the change of Cs retention performance by framework damage. Concentration of cesium in solution leached was estimated by atomic absorption spectrophotometry.

RESULTS: All the XRD patterns of powders prepared were demonstrated that they were pollucite, and all the patterns showed that they contained only single-phase pollucite.

In our previous study, the irradiated pollucite sample showed little difference from the non-irradiated one in the amount of leached cesium. Then we concluded that frameworks were not destroyed by ^{60}Co-irradiation. However, we found some questions about PCT-A method, then the leaktests were studied again.

It was estimated that amount of leached cesium from samples with and without ^{60}Co-irradiation. Over 45 ppm Cs were measured in most samples regardless of whether irradiated or not, and these values of Cs concentration measured were quite higher than those measured by other researchers[5]. It is considered that the reason why the concentration of cesium ions leaked from pollucite was high to be insufficient washing and cesium adsorbed on the ion exchange site.

REFERENCES:

[1] Y. Yokomori *et al.*, *Sci. Rep.*, **4** (2014), 4195
[2] J. Fortner *et al*., Argonne National Laboratory, Argonne, Illinois 60439 (2001).
[3] N. J. Hess *et al.*, *J. Nucl. Mater.*, **281** (2000), 22-33.
[4] ASTM C 1285-02 (2008).
[5] Z. Jing *et al.*, *J. Hazard. Mater.*, **306** (2016), 220–229.

CO4-26 Defect Structure with Short Positron Lifetime in Tungsten

A. Yabuuchi

Institute for Integrated Radiation and Nuclear Science, Kyoto University

INTRODUCTION: The calculated positron lifetime for a monovacancy in tungsten has been reported to be 193 ps−200 ps [1−3]. The positron lifetime of tungsten irradiated with p^+ or $^3He^+$ in a vacuum has been observed experimentally to be 190 ps−200 ps [4−6]. However, the positron lifetime of tungsten irradiated with electrons in coolant water has been reported to be around 170 ps, which is shorter than the calculated positron lifetime for a monovacancy [3,7,8], and the reason for this is unclear. In this study, positron lifetime measurements of electron-irradiated tungsten and first-principles calculations of positron annihilation properties were conducted.

EXPERIMENTS: Tungsten samples with a purity of 99.999% (5N) were annealed at over 2273 K in a vacuum before irradiation. After the annealing, 8 MeV electrons were irradiated to the samples at around 373 K using the KURNS-LINAC with total doses of 5×10^{19} e^-/cm^2. Positron annihilation lifetime measurements were performed at room temperature.

CALCULATIONS: The calculations were performed using ABINIT 8.10.3 [9], a first-principles electronic structure calculation code based on density functional theory (DFT). The Perdew-Burke-Ernzerhof (PBE) electron-electron exchange-correlation functional [10] and Blöchl's projector augmented wave (PAW) method [11] were used. Positron annihilation calculations were performed with a two-component DFT calculation scheme [12] using the Puska-Seitsonen-Nieminen (PSN) [13] local density approximation as the electron-positron exchange-correlation functional. A computational cell size of 3×3×3 (54 atoms of perfect crystal) was used, and the cutoff energy of the plane wave was set to 408 eV.

RESULTS: In the present study, a positron lifetime of about 170 ps was experimentally observed from electron-irradiated tungsten. On the other hand, the calculation of this work also indicated that the positron lifetime for monovacancy (*V*) is 195 ps, which is comparable to the previous studies. The calculated positron lifetimes of the defect complexes such as *V*-2H, *V*-C, *V*-N, and *V*-O were all around 170 ps. This is comparable to the experimentally observed positron lifetime. In addition, the calculated annihilation gamma-ray Doppler broadening spectra of *V*-2H and *V*-O showed different spectral shapes, indicating that at least *V*-2H and *V*-O can be distinguished from the Doppler broadening measurements.

REFERENCES:

[1] T. Troev *et al.*, Nucl. Instrum. Methods Phys. Res. Sect. B **267** (2009) 535.
[2] P. Staikov, N. Djourelov, Phys. B **413** (2013) 59.
[3] K. Sato *et al.*, J. Nucl. Mater. **496** (2017) 9.
[4] P. E. Lhuillier *et al.*, Phys. Status Solidi C **6** (2009) 2329.
[5] O. V. Ogorodnikova *et al.*, J. Nucl. Mater. **517** (2019) 148.
[6] O. V. Ogorodnikova *et al.*, J. Nucl. Mater. **525** (2019) 22.
[7] T. Toyama *et al.*, J. Nucl. Mater. **499** (2018) 464.
[8] K. Sato *et al.*, Nucl. Mater. Energy **9** (2016) 554.
[9] X. Gonze *et al.*, Comput. Phys. Commun. **205** (2016) 106.
[10] J. P. Perdew *et al.*, Phys. Rev. Lett. **77** (1996) 3865.
[11] P. E. Blöchl, Phys. Rev. B **50** (1994) 17953.
[12] J. Wiktor *et al.*, Phys. Rev. B **87** (2013) 235207.
[13] M. J. Puska *et al.*, Phys. Rev. B **52** (1995) 10947.

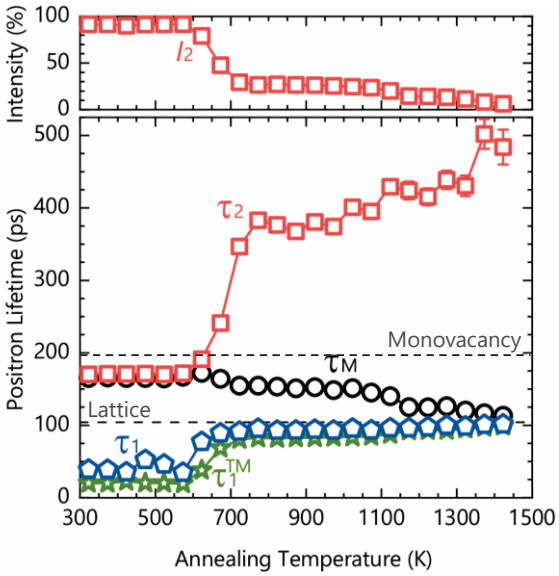

Fig. 1. Annealing behavior of positron lifetime in electron-irradiated tungsten. Lower and upper dashed lines indicate positron lifetimes for perfect lattice and monovacancy, respectively.

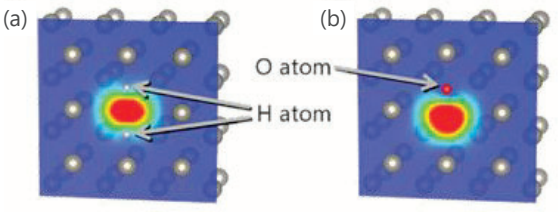

Fig. 2. Calculated atomic configuration and positron density distribution of the defect complexes. (a) *V*-2H, (b) *V*-O.

CO4-27 Elucidation of the Mechanism of the Screw-sense Induction and Helix Inversion of Polymer Main Chain Based on the Small Angle X-ray Scattering, the Dynamic Light Scattering, and the Quasielastic Neutron Scattering Measurements

Y. Nagata[1], M. Suginome[2], M. Sugiyama[3], R. Inoue[3], N. Sato[3], and K. Morishima[3]

[1] *Institute for Chemical Reaction Design and Discovery, Hokkaido University*
[2] *Graduate School of Engendering, Kyoto University*
[3] *Institute for Integrated Radiation and Nuclear Science, Kyoto University*

INTRODUCTION: Much attention has been paid to the structural control of helical polymers owing to their potential applications for asymmetric catalysts, chiral stationary phase, and chiroptical materials. Recently, we have reported that helical poly(quinoxaline-2,3-diyl)s (PQXs) bearing chiral side chains exhibit solvent-dependent helix inversions,[1-3] which can serve as effective scaffold for chirality-switchable materials. [4-7] In order to elucidate the mechanism of the screw-sense induction and the helix inversion of PQXs, we have investigated the detailed structures of a PQX (100mer) with right- or left-handed structures in tetrahydrofran-d_8 (THF-d_8) or a mixed solvent of 1,1,2-trichloroethane-d_3 (1,1,2-TCE-d_3) and THF-d_8 (4/1, v/v) by using small-angle neutron scattering (SANS) experiments, in conjunction with theoretical calculations.[8] The obtained structures of the PQX suggested that the right-handed structure in THF-d_8 is well solvated, while the left-handed structure in 1,1,2-TCE-d_3/ THF-d_8 (4/1, v/v) is less solvated.

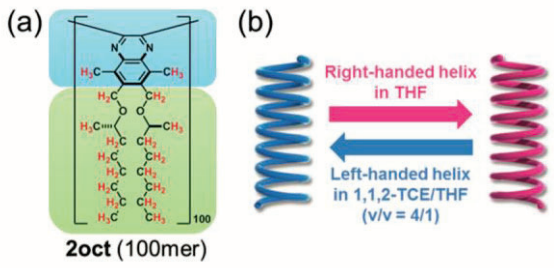

Figure 1. (a) the molecular structure of the PQX bearing (*R*)-2-octyloxymethyl side chains. (b) Solvent-dependent helix inversion of the PQX.

Our recent interest has focused on the effect of the dynamics of the side chains on the screw-sense induction. So far, we have carried out quasielastic neutron scattering (QENS) measurements to elucidate the impact of the molecular dynamics on the solvent-dependent helix inversion of the PQX. In this study, we have carried out QENS measurements and dynamic light scattering (DLS) measurements for the detailed analysis of the results of the QENS measurements.

EXPERIMENTS: A PQX bearing (*R*)-2-octyloxymethyl side chains (100mer) was prepared according to our previous paper.[2] The QENS measurements were carried out at BL-02 DNA in J-PARC. The light scattering measurements were carried out with a 22-mW He-Ne laser, an Avalanche Photo Diode (APD, ALV, Germany) mounted on static/dynamic compact goniometer, ALV/LSE-5003 electronics, and ALV-5000 Correlator (ALV-Laser Vertriebsgesellschaft GmbH, Langen, Germany). The measurements were performed at 313 K and CONTIN analysis was used to obtain the probability of decay rate at each Q.

RESULTS: The PQX was dissolved in THF-d_8 or a mixed solvent of 1,1,2-trichloroethane-d_3 (1,1,2-TCE-d_3) and THF-d_8 (4/1, v/v), respectively, to carry out DLS measurements. In both cases, the decay constant Γ and the square of the wave vector q^2 showed linear relationship, affording the diffusion constants in these solvents. We are now working on the analysis of the QENS measurements by using the results of the DLS measurements. In addition, we are now trying to reveal the detailed behavior of the screw-sense induction and the helix inversion using molecular-dynamics simulations using the BIOVIA Materials Studio with the COMPASS II force field.

REFERENCES:

(1) Yamada, T.; Nagata, Y.; Suginome, M. *Chem. Commun.* **2010**, *46*, 4914-4916.
(2) Nagata, Y.; Yamada, T.; Adachi, T.; Akai, Y.; Yamamoto, T.; Suginome, M. *J. Am. Chem. Soc.* **2013**, *135*, 10104-10113.
(3) Nagata, Y.; Nishikawa, T.; Suginome, M. *J. Am. Chem. Soc.* **2015**, *137*, 4070-4073.
(4) Nagata, Y.; Nishikawa, T.; Suginome, M. *Chem. Commun.* **2012**, *48*, 11193-11195.
(5) Nagata, Y.; Takagi, K.; Suginome, M. *J. Am. Chem. Soc.* **2014**, *136*, 9858-9861.
(6)Nagata, Y.; Uno, M.; Suginome, M. *Angew. Chem. Int. Ed.* **2016**, *55,* , 7126-7130.
(7) Nishikawa, T.; Nagata, Y.; Suginome, M. *ACS Macro Lett.* **2017**, *6*, 431-435.
(8) Nagata, Y.; Nishikawa, T.; Suginome, M.; Sato, S.; Sugiyama, M.; Porcar, L.; Martel, A.; Inoue, R.; Sato, N. *J. Am. Chem. Soc.* **2018**, *140*, 2722-2726.

CO4-28 Neutron irradiation tests for ITER plasma diagnostics

M. Ishikawa, E. Yatsuka, R. Imazawa, T. Ushiki, H. Murakami and T. Hatae

National Institutes for Quantum and Radiological Science and Technology

INTRODUCTION: International Thermonuclear Experimental Reactor (ITER) [1] is being built in France by international cooperation. This study focuses on neutron irradiation effects on optical elements and piezo-actuators used in ITER. Expected 1 MeV Silicon equivalent fluence is 10^{12}-10^{15} n/c m^2 depending on locations of components. In order to investigate the effect of such high fluence on the actual components in a short time, neutron irradiation was performed using the slant exposure tube and the pneumatic tubes of the KUR. This report mainly presents effect of neutron irradiation on piezo actuators for Poloidal Polarimeter (PoPola) system and briefly describes the tests for other systems such as Edge Thomson Scattering system (ETS), Infrared Thermography (IRTh) system and the Microfission Chamber system (MFC).

The authors carried out the irradiation test of a piezo actuator. Piezo actuators will be used in various systems of ITER and will be used for adjustment of mirror angle in the case of PoPola. The previous study [2] assessed radiation hardness of a piezo actuator for other system of ITER and shows that the piezo actuator is operational in the ITER radiological environment. However, since the piezo actuator selected for PoPola is different from that used in the previous study, the authors need to conduct an irradiation test of the piezo actuator of PoPola to confirm whether it can be used in the ITER environment.

EXPERIMENTS: At the place where the piezo actuator was placed in the slant exposure tube of KUR, the neutron flux is 9.6x10^{11} (n/cm^2/s), the cadmium ratio is 34.0, and the gamma flux is 50 (kGy/h). The duration of irradiation was one hour in total, so the total neutron flux was 3.5x10^{15} (n/cm2), which is equivalent to the expected fluence at the position of the PoPola piezo actuator in ITER.

The tested piezo actuator was PZA 12 released by Newport Company. The motion of the piezo actuator is as discrete as that of a stepping motor. The driver of the piezo actuator sends polyphase voltage signals to the piezo actuator, and then the shaft of the piezo actuator moves in discrete steps. The aims of this test are as follows;

- To confirm whether the stroke force of the piezo actuator is over 25 N.
- To confirm whether the maximum stroke length of the piezo actuator is over 7.4 mm.

The values of 25 N and 7.4 mm come from mechanical and optical design of the PoPola system. It should be noted that the stroke length per step is not important because the mirror angle is controlled in a closed loop using both the mirror angle sensor and the piezo actuator. Thus, what is important for PoPola is that the piezo actuator can travel the distance of 7.4 mm or more with the stroke force of 25 N or more after irradiation.

Figure 1 shows the schematics and the photograph of the device that the authors developed for this test. The test device always applies axial load of 45 N to the piezo actuator during the test by using constant force springs (Sunko, model: NWS 1.5-1). The axial load can be changed by exchanging the constant force springs. The motion of the piezo actuator is monitored by a micrometer (Mitsutoyo Corporation, model: 2050S, minimum scale division: 10 μm).

RESULTS: The functional test was conducted after the neutron irradiation. By using the device shown in Fig. 1, the authors confirmed that the piezo travel the distance of 10 mm or more with the stroke force of 45 N. Thus, it can be concluded that the selected piezo actuator has radiation hardness enough for PoPola in the ITER environment.

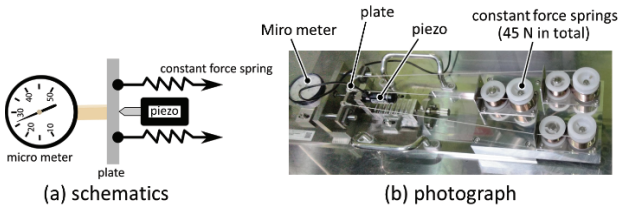

Fig. 1: Functional test device of piezo actuator.

ON GOING INVESTIGATIONS AND PROSPECTS:

RETS will use a silica core optical fiber to transmit scattered light from plasma to the spectrometer. If the silica core contains a large amount of OH groups, it becomes resistant to deterioration of light transmittance due to neutron irradiation in the visible light, but absorption occurs regardless of irradiation in the near infrared. Experiments are on-going to investigate the relationship between OH group content and spectral transmittance.

IRTh will use Au coating mirrors, AR coated sapphire vacuum windows and several lens materials in the ITER environment. In order to investigate threshold value of the total dose for keeping their optical performances, irradiation tests of several candidate materials for mirror, windows and lens have been conducted since 2019. Then, the they will be completed by 2021. In 2020, irradiation tests for several kinds of materials for mirrors and windows were conducted and threshold values of those materials are being investigated.

The feedthrough of MFC plays an important role for vacuum and tritium confinement of the ITER vacuum vessel. However, ceramic material used in the feedthrough may suffer damage due to high neutron irradiation and it could cause leakage of vacuum and tritium. In order to demonstrate radiational hardness of the feedthrough, equivalent neutron fluence to that at the location of the feedthrough in ITER was irradiated. The leak test of the ceramic part will be carried out to confirm its confinement function in 2021.

REFERENCES:

[1] B. Bigot, Fusion Eng. Des., **146**, 124 (2019).
[2] M. Pillon *et al*., Fusion Eng. Des., **96-97**, 329 (2015).

CO4-29 Irradiation Experiment of Accident Tolerant Control Rod Materials (2)

H. Ohta[1], K. Nakamura[1], Y. Takahashi[2], H. Unesaki[2], T. Sano[2*]
[1]*Nuclear Research Technology Laboratory, Central Research Institute of Electric Power Industry*
[2]*Institute for Integrated Radiation and Nuclear Science, Kyoto University*
[*]*Present affiliation: Atomic Energy Research Institute, Kindai University*

INTRODUCTION: Various concepts of "enhanced-accident tolerant fuels and core components" have been developed in many countries to improve core safety under any operation conditions including severe accidents (SAs), while maintaining or improving the economic efficiency of light water reactors (LWRs). The Central Research Institute of Electric Power Industry (CRIEPI) has been developing the accident tolerant control rods (ATCRs) where the novel neutron absorbing materials including rare-earth oxides (RE_2O_3) are applied[1] to prevent control rods (CRs) from damaging prior to fuel rods in the early stages of SAs. Preliminary analyses[1] revealed the ATCR concept improves the reactor shutdown margin and neutronic lifetime. RE_2O_3 (RE = Sm or Eu) has excellent high temperature compatibility with the stainless steel CR cladding and will not be damaged less than 1200 °C. On the other hand, it is known to have extremely high hygroscopicity and is unstable, but it was experimentally confirmed that physicochemical stability is improved even under high temperature steam atmosphere by mixing and sintering with MO_2 (M = Zr or Hf)[2]. In addition, thermal neutron irradiation characteristics of the mixtures of RE_2O_3-MO_2 are needed to be confirmed to evaluate the applicability as a control rod for LWRs. In this study, dimensional stability of a candidate material by neutron irradiation will be confirmed.

EXPERIMENTS and RESULTS

Sample Preparation: The powders of Sm_2O_3 and ZrO_2 were mechanically mixed at a molar ratio of 1 : 1 and sintered to form a pellet with a density of 6.55 g/cm^3 corresponding to 93.7 %TD. Since the sintered mixtures of any combinations of RE_2O_3-MO_2 (RE = Sm or Eu, M = Zr or Hf) with a molar ratio of 1 : 1 is known to form a fluorite crystal structure, it is considered that the irradiation experimental results of Sm_2O_3-ZrO_2 are applicable to the other combination materials. For minimizing the radioactivation induced by the neutron irradiation, the sintered pellet was cut into small pieces. The appearance and surface microstructure of the cut sample pieces before irradiation was observed with an optical microscope and scanning electron microscope (SEM), and their weights were measured.

Irradiation Conditions: Irradiation experiment has been carried out using long-term irradiation plug in Kyoto University Research Reactor (KUR). Three Sm_2O_3-ZrO_2 sample pieces were enclosed in an Al capsule dedicated for long-term irradiation experiment and irradiated for 254.7 hours at a rated power of 1 MW and 55.2 hours at a high power of 5 MW at 85 - 90 °C. The fast and total neutron fluences at the end of irradiation experiment are estimated to be 5.35×10^{18} n/cm^2 and 2.38×10^{19} n/cm^2, respectively, which is almost equivalent to irradiation fluence for ~1 day in typical PWRs.

Postirradiation observations: After ~2 years cooling, the appearances and surface microstructure of the irradiated samples were observed, and their weights were also measured. The weight change before and after irradiation was within ± 1.0% and not remarkable, as shown in Table I. Figure 1 shows the appearance of each sample before and after irradiation. No changes in the appearance and the dimensions due to neutron irradiation were confirmed. Furthermore, the microstructure on the surface of the irradiated samples observed with SEM showed no sign of change as compared with the unirradiated sample as shown in Figure 2.

Table I Weight changes of Sm_2O_3-ZrO_2 samples before and after irradiation[3].

Sample No.	(1)	(2)	(3)
Before irrad.	1.95 mg	6.21 mg	5.15 mg
After irrad.	1.97 mg	6.15 mg	5.11 mg

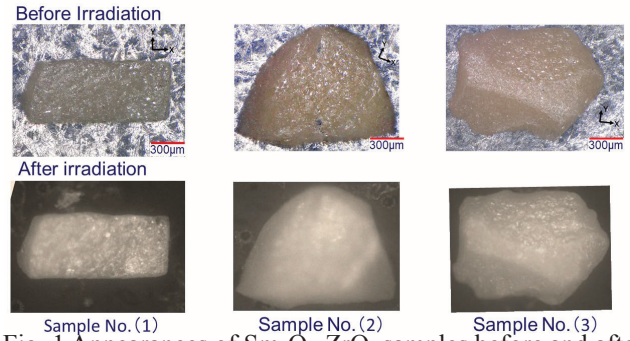

Fig. 1 Appearances of Sm_2O_3-ZrO_2 samples before and after irradiation [3].

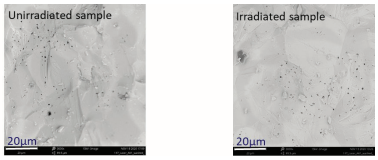

Fig. 2 SEM images of Sm_2O_3-ZrO_2 samples before and after irradiation[3].

CONCLUSION: Irradiation experiment of sintered Sm_2O_3-ZrO_2 samples in long-term irradiation plug of KUR showed that the irradiation stability of the ATCR neutron absorbers was maintained under a fast neutron fluence of 5.35×10^{18} n/cm^2.

REFERENCES:

[1] H. Ohta, et al., TopFuel 2016, 17556 (2016).
[2] K. Nakamura, et al., *AESJ 2017 spring meeting*, 1I06.
[3] H. Ohta et al., *AESJ 2021 spring meeting*, 2K02.

CO4-30 Radiochemical Research for the Advancement of $^{99}Mo/^{99m}Tc$ Generator by (n, γ) Method (3)

Y. Fujita, M. Seki, Y. Namekawa, K. Nishikata, F. Daigo, H. Ide, K. Tsuchiya, T. Sano[1], Y. Fujihara[2], J. Hori[2], H. Yoshinaga[2]. J. Zhang[2], T. Suzuki[3] and H. Suematsu[3]

Department of JMTR, Japan Atomic Energy Agency
[1] Atomic Energy Research Institute, Kindai University
[2]Institute for Integrated Radiation and Nuclear Science, Kyoto University
[3]Graduate School of Engineering, Nagaoka University of Technology

INTRODUCTION: The research and development (R&D) has been carried out for the production of Molybdenum-99 (^{99}Mo) by the neutron activation method ((n, γ) method) from viewpoints of limited availability of high-enriched uranium, no-proliferation and nuclear security and disposal of nuclear fissile materials. The amount of ^{99}Mo to be produced by (n, γ) reaction is very low. Thus, the solvent extraction was applied as a Master-Milker in order to increase the concentration of ^{99m}Tc in the final product [1]. This method employs MEK to extract ^{99m}Tc from ^{99}Mo. In this study, the extraction property of ^{99m}Tc was evaluated using the Mo solution with irradiated MoO_3 by MEK and characterization of ^{99m}Tc solution was performed by the column chromatography after the extraction of ^{99m}Tc. Additionally, high-density MoO_3 pellets irradiated with KUR were transported to JMTR-HL, and the similar experiments were conducted as a scale-up test.

EXPERIMENTS: The MoO_3 pellet pieces (about 1.5 g) were irradiated in the condition of 20min×5MW in the Pn-2 of the KUR. After the irradiation, the irradiated MoO_3 pellet pieces were dissolved with 6M-NaOH solution (3.75 mL) and mixed with other Mo solution dissolved un-irradiated MoO_3 powder (33 g) and 6M-NaOH (85 mL). Two kinds of Mo solution samples were prepared. One is the Mo solution (hereinafter referred to as "MoSol-A") containing water (8mL). The other is the Mo solution (hereinafter referred to as "MoSol-B") containing water (6 mL) and saline (2 mL). MEK was added to each Mo solution, only MEK was extracted after stirring. The extracted MEK was purified using the basic alumina columns, and ^{99m}Tc in MEK was adsorbed using the acidic alumina column. The ^{99m}Tc was eluted from the acidic alumina column with saline of 10 mL. Radioactivity in Mo solution and Tc solution in each step was measured by the γ-ray spectrometer.

RESULTS: Fig.1 shows the ^{99m}Tc content in medium of each step. The ^{99m}Tc content is the ratio of the amount of ^{99m}Tc contained in medium to the amount of ^{99m}Tc in the Mo solution at the start of extraction. The ^{99m}Tc radioactivity was corrected at the start of extraction. In the experiment using Mo solution of MoSol-A, the ^{99m}Tc content was stable until the adsorption step of acidic alumina column. In the experiment using Mo solution of MoSol-B, the ^{99m}Tc content was reduced at the extraction step from Mo solution of MoSol-B at the first day. On the other hand, the ^{99m}Tc content was stable until the adsorption step of acidic alumina column at the 2nd and 3rd days. It seems that the extraction of ^{99m}Tc by MEK is affected by Cl^- ion contents in the Mo solution. At the elution step from the acidic alumina column, ^{99m}Tc elution amount reduced in all cases. The cause may be the preparation method and filling amount of the acidic alumina, the elution rate, etc. The effects from them need to be investigated and improved.

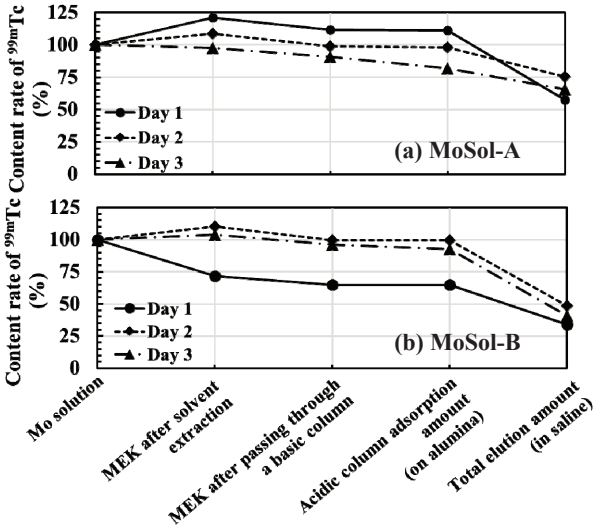

Fig.1 ^{99m}Tc content in medium of each step.

Fig.2 shows ^{99m}Tc elution fraction from the acidic alumina column. As a result, it was found that the elution property was the same tendency in all cases and that almost 100% of ^{99m}Tc could be eluted with about 4 mL of saline.

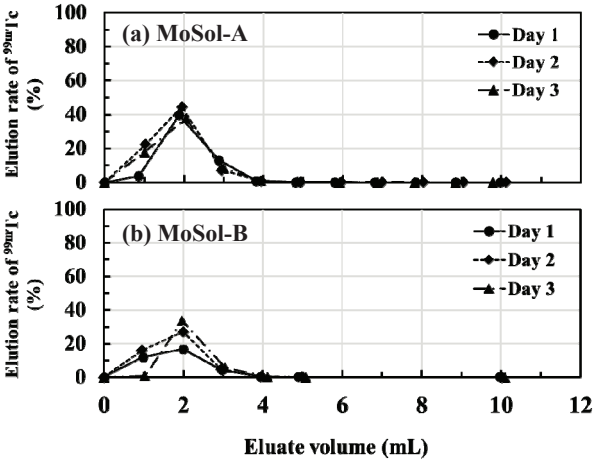

Fig.2 ^{99m}Tc elution fraction from the acidic alumina column.

REFERENCES:

[1] S. Chattopadhyay *et al.*, Appl. Radiat. Isot., **68** (2010) 1–4

CO4-31 The Absorbance Measurement for Color Dosimeter of Gamma-ray Using a Photochromic Diarylethene Containing Additives

S. Komatsuda, M. Takeshita[1], R. Maeda[1], A. Taniguchi[2], and Y. Ohkubo[2]

Institute of Human and Social Sciences, Kanazawa University
[1]*College of Human and Social Sciences, Kanazawa University*
[2]*Institute for Integrated Radiation and Nuclear Science, Kyoto University*

INTRODUCTION:

Diarylethene (DAE) is one of the most intriguing photochromic materials which has a reversibly structure-changed part by irradiating ultraviolet (UV) ray or gamma ray. The DAE is colored by this structural change and returned to original structure by irradiating visible rays. Because of their excellent thermostability and reversibility, the DAE has attracted much attention as radiation-induced color dosimeter. In addition, for practical use of DAE, a sensitizer such as aromatic compound is contained with DAE to enhance sensitivity.

It was found from previous studies that a DAE containing aromatic compound was colored visually by irradiating gamma-ray of 100 Gy[1]. However, for practical use of DAE as color dosimeter, it is necessary to obtain highly sensitive DAE colored by irradiating gamma-ray of 0.1~1 Gy. Therefore, it is required to obtain more information on suitable sensitizer of aromatic compound for DAE color dosimeter. For that purpose, we then study the sensitizing effect of various aromatic compounds contained in DAE solution, observing the absorption spectra of DAE irradiated by gamma-ray.

EXPERIMENTS: A measuring sample is constituted of a toluene solution containing diarylethene(concentration of 2.6×10^{-3} mol/L) and an additive(concentration of 2.6×10^{-3} mol/L). Commercially available 1,2-bis(2,4-dimethyl-5-phenyl-3-thienyl)-3,3,4,4,5,5-hexafluoro-1-cyclopentene (DAE) and additives such as naphthalene, anthracene, biphenyl, and *p*-terphenyl were dissolved in toluene solution, respectively. The solutions were dispensed into vials and irradiated at room temperature with Co-60 Gamma-ray Irradiation Facility at Institute for Integrated Radiation and Nuclear Science. The irradiation dose of gamma-ray was 361 Gy. The absorbance measurements were carried out with JASCO V-570.

RESULTS: Figure 1 shows the absorption spectra of irradiated DAE samples. Table 1 summarizes the maximum absorption wavelength λ_{max} of the DAE at 575 nm. The absorption peaks of the samples are increased by containing additives compared with sample without additives, which exhibits that the additives of aromatic compounds have the sensitizing effect. Especially, biphenyl and *p*-terphenyl have a high sensitizing effect. Focusing on λ_{max} and quantum yield of additives, there are two common features for effective additives of aromatic compound; (i) for one thing, λ_{max} of additives is about 265 nm, and (ii) for other thing, the additives show high quantum yield. In order to corroborate this proposal, we performed additional preliminary experiment measuring UV irradiated DAE samples for examining the sensitizing effect of another additives (such as *p*-xylene, phenylacetylene, and anisole) which shows high quantum yield and λ_{max} at about 265 nm. For the result of this additional experiment, it is suggested that the sensitizing effect of anisole is nearly equals to biphenyl which shows the best sensitizing effect in this work. This observation is consistent with our proposal on the sensitizing effect of additives. For more information on the condition of effective additives, additional experiments using gamma-ray is now in progress.

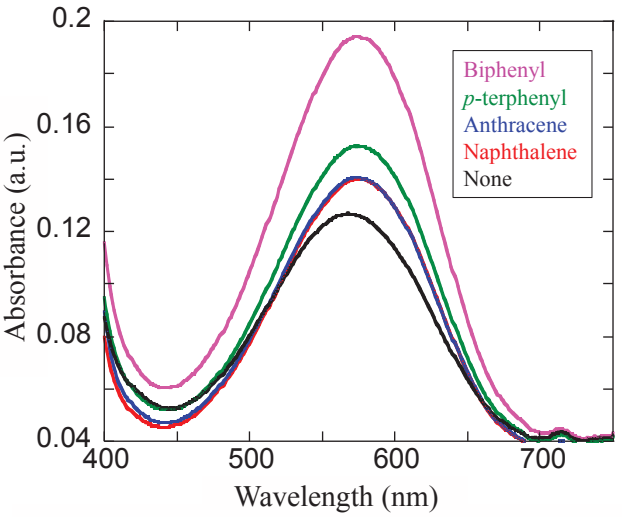

Fig. 1. Absorption spectra of DAE samples in toluene solution.

Table 1 Measured absorbance at 575 nm of samples irradiated by Co-60 gamma-ray

Additives	Absorbance at 575 nm	λ_{max} of additives (nm)	Fluorescence quantum yield of additives
None	0.12	—	—
Naphthalene	0.14	286	0.23
Anthracene	0.14	358	0.36
Biphenyl	0.19	247	0.18
p-terphenyl	0.15	276	0.80

REFERENCES:

[1] S. Irie *et al.*, *The Chem. Soc. Jpn.* **75** (2002) (2071-2074).

Synthesis and superconducting properties of $EuSn_2As_2$

***R. Takahashi*[1], *Y. Tani*[1], *N. Nagasawa*[1], *S. Ikeda*[1], *N. Kawamura*[2], *K. Mimura*[3], *A. Yamaguchi*[1], *A. Sumiyama*[1], *H. Kobayashi*[1], *H. Wadati*[1]**

[1]*Graduate School of Material Science, University of Hyogo, Ako, Hyogo 678-1297, Japan*
[2]*Japan Synchrotron Radiation Research Institute (JASRI), Sayo, Hyogo 679-5198, Japan*
[3]*Graduate School of Engineering, Osaka Prefecture University, Sakai 599-8531, Japan*

INTRODUCTION: $EuSn_2As_2$ is one of the two-dimensional stacked van der Waals materials which providing attractive platform to realize various properties by changing the element, temperature and pressure [1, 2]. Recently, it has been reported that this material exhibits abnormal superconductivity, and its origin is urgently elucidated. The point of particular attention is that while the superconducting state in the ab direction is realized, the resistance does not become zero in the c direction, which is thought to be due to the Josephson junction with the Eu layer as the insulating layer, however, it is unclear [2]. This time, we focused on the electronic state of the Eu layer and tried to identify its valence state.

EXPERIMENTS: The sample was prepared by the Sn-flux method [1]. Samples were evaluated using laboratory X-Ray Diffractometer (Cu-Kα) and Energy Dispersive X-ray Spectroscopy. Since the crystallinity and composition were highly dependent on the sample, the one with the lattice constant closest to the previous study[1] and the composition closest to Eu: Sn: As = 1: 2: 2 was selected from the measured samples, and the single crystal $EuSn_2As_2$ sample was selected. Then, magnetization measurement, resistivity measurement, and specific heat measurement were performed using PPMS and MPMS-5SH (Quantum design). We also performed high energy resolution fluorescence detected X-ray absorption fine structure spectroscopy measurements on SPring-8 BL39XU at T = 2.7, 300 K to identify the valence state of Eu.

RESULTS: From the measurement of magnetization, the effective magnetic moment was found to be 7.337 μ_B/Eu [Fig. 1 (b)] slightly lower than that of theoretical value 7.94 μ_B/Eu^{2+} (J = 7/2) and Meissner effect was observed at 3.7 K (B = 0.5 mT). We also measured Eu-L_3 edge High Energy Resolution Fluorescence Detected X-ray Absorption Fine Structure (HERFD-XAFS) spectroscopy for the $EuSn_2As_2$ single crystal [Fig. 1 (c)]. Only Eu^{2+} peak was observed at both 300 K and 3 K and there was no Eu^{3+}. We would like to discuss the difference between magnetic properties and valence of Eu, and superconducting properties of $EuSn_2As_2$.

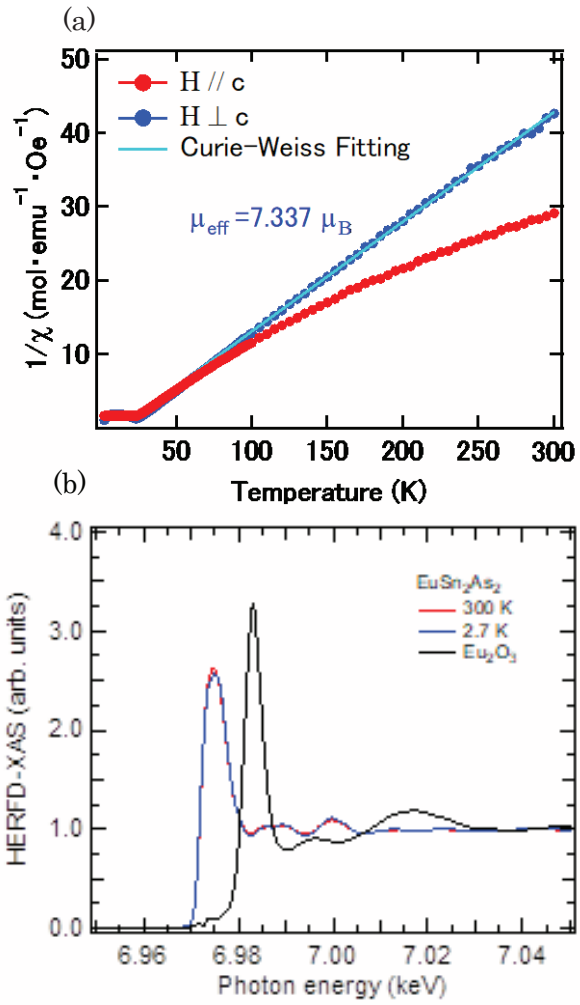

Fig. 1. (a) Magnetic susceptivity of $EuSn_2As_2$. (b) HERFD-XAFS spectra.

REFERENCES:

[1] H. Li *et al.*, Phys. Rev. X **9**, 041039 (2019).
[2] S. Sakuragi *et al.*, arXiv:2001.07991.